JOURNAL OF CATALYSIS 156, 185–207 (1995)

Activation of Precipitated Iron Fischer–Tropsch Synthesis Catalysts

Mehul D. Shroff,* Dinesh S. Kalakkad,* Kent E. Coulter,† Steven D. Köhler,† Mark S. Harrington,† Nancy B. Jackson,† Allen G. Sault,† and Abhaya K. Datye[1,*]

*Department of Chemical and Nuclear Engineering and UNM/NSF Center for Microengineered Ceramics, University of New Mexico, Albuquerque, New Mexico 87131; and †Process Research Department, M.S. 0709, Sandia National Laboratories, Albuquerque, New Mexico 87185-0709

Received January 31, 1995; revised April 14, 1995; accepted June 7, 1995

The effect of activation and reaction treatments on the resulting phase transformations in a commercial, precipitated, and spray-dried Fe_2O_3–CuO–K_2O Fischer–Tropsch catalyst has been studied. The catalyst was activated in flowing H_2, CO, and a H_2/CO = 0.7/1.0 mixture. The pretreatment method caused these catalysts to exhibit significant differences in their catalytic activity for CO hydrogenation. The microstructure of these catalysts was studied by electron microscopy and other bulk and surface characterization techniques to understand the phenomena responsible for these differences. We observe that magnetite transforms into carbide as the catalyst is activated, causing the crystals of magnetite to break down into smaller crystallites of the carbide phase. Deposition of carbon on the carbide surface causes the carbide crystallites to further separate from each other. Our results suggest that magnetite has negligible catalytic activity for FT synthesis whereas carbide formation is necessary before the catalyst becomes active. The extent of transformation into carbide correlates well with catalyst activity during the activation step.

INTRODUCTION

Depleting oil reserves make it necessary to develop alternative methods for synthesizing hydrocarbon fuels. The Fischer–Tropsch (FT) synthesis, first developed in Germany in 1923 (1), is an important step in the indirect liquefaction of coal. The original process was carried out with iron filings promoted with potassium. The current generation of catalysts includes cobalt and ruthenium as well as iron promoted by copper, potassium, and other oxides (2). The interest in use of iron for FT synthesis stems from its water–gas shift activity as well as its easy availability and low cost, which promote economy of operation. Iron catalysts can be used in a fixed bed, or in a slurry phase fluidized bed, depending on the desired product mix and operating pressure and reaction conditions. A serious problem in the use of iron catalysts in the slurry process is their tendency to undergo attrition (3) during use. This can cause fouling of downstream equipment as well as making the separation of catalyst from product wax virtually impossible (4).

The Group VIII metals (Co, Ni, Ru, Fe) which are the most common FT synthesis catalysts are generally synthesized in the form of a metal oxide. Consequently these catalysts must be subjected to an activation treatment before the catalysts become active for Fischer–Tropsch synthesis. Cobalt, nickel, and ruthenium are almost always reduced in flowing H_2 at temperatures between 473 and 723 K and remain in the metallic state during synthesis (2) under a variety of process conditions. However, the picture is not so clear in the case of iron catalysts where it has been variously speculated that the oxide (magnetite) (5, 6) or the iron carbide (7) may constitute the active phase. Part of the confusion stems from the fact that the nature and composition of the iron catalyst undergoes changes during reaction. These changes depend on the temperature, time of exposure to the reactant feed, nature of the reactor system, composition of the feed and activation conditions (time and temperature). The common pretreatment conditions employed in the case of iron catalysts are H_2 reduction, CO reduction, or reduction in the reactant gas (induction). A calcination step may precede the reduction of the catalyst (2). In this paper, we describe the effects of pretreatment on a commercial precipitated iron catalyst. We have also studied the effect of performing FT synthesis with a H_2/CO 0.7:1 syngas feed at 523 K.

Several phases of iron are known to exist when iron-based catalysts are subjected to FT synthesis conditions (8–11). These include metallic iron (α-Fe), iron oxides (hematite, α-Fe_2O_3; magnetite, Fe_3O_4 and Fe_xO), and iron carbides, of which at least five different forms are known to exist. These include O-carbides (carbides with carbon atoms in octahedral interstices, ε-Fe_2C, ε'-$Fe_{2.2}C$, and Fe_xC), and TP-carbides (carbides with carbon atoms in trigonal prismatic interstices, χ-$Fe_{2.5}C$ and Fe_3C). The formation and distribution of these phases depends on the reaction conditions, reaction times, and state of the catalyst

[1] To whom correspondence should be addressed.

0021-9517/95 $12.00

(reduced/unreduced, supported/unsupported, etc.). However, the role of each of these phases during the reaction has not been resolved.

In 1982, Teichner and co-workers (5, 6) proposed that magnetite was the active phase. This assertion was questioned in 1986 by Dictor and Bell (12), whose results support the proposal that the active phase is a mixture of χ- and ε'-carbides and some metallic α-Fe. The debate over whether magnetite is the active phase has been revived in recent years by Kuivila *et al.* (13), who suggest that magnetite is the active phase. In a series of review articles, Butt (14, 15) asserts that magnetite may be active for reaction in the absence of carbide phases. In our opinion, there are two possible explanations for the controversy surrounding the role of the magnetite phase: First, magnetite may form on the catalyst surface as it is passivated after reaction (both O_2 in ambient air or H_2O in the reaction products might serve as the oxidizing agent). Second, the carbide phase is difficult to detect by techniques such as X-ray photoelectron spectroscopy (XPS) and X-ray diffraction (XRD), as we shall show in this paper. This is particularly evident in a recent paper by Huang *et al.* (16), who found by XRD that magnetite was the only crystalline phase when the catalyst had reached its peak activity. However, the magnetite catalyst was inactive when it was initially exposed to syngas. They therefore conclude that magnetite is not necessarily the active phase. They suggest the possibility that a surface phase on the magnetite may be the active phase, but XRD does not provide any direct evidence for this hypothesis. Similarly, Teichner and co-workers (5, 6) find that the proportion of magnetite falls continuously as a function of time, while the catalyst activity first increases and then decreases over the same time interval. All of these results suggest that the active phase formed by the reduction of the magnetite may be difficult to detect by bulk techniques, resulting in a controversy on the role of the magnetite in the FT synthesis.

There have been two models with regard to the role of the carbide phase. In the carbide model (7), catalytic activity is thought to be due to active surface sites located on the bulk carbide phase and site density is shown to follow the extent of bulk carbidization (7). A second model, the competition model (11), proposes that activity is due to surface iron atoms and there is competition for the CO molecules between bulk carbidization and hydrocarbon formation. This model is based on the observation (8, 11) that metallic iron is not initially active but rapidly undergoes carbidization, while the catalytic activity increases gradually and then declines as the catalyst gets completely transformed into the carbide. It is possible that the transformation of the metal into carbide results in an increase in activity while the decline could be due to the deposition of inactive carbon on the active carbide surface. The nature of the carbon may also be important; for example, amorphous carbon may not deactivate the catalyst as much as graphitic carbon. Only a technique with adequate spatial resolution that can distinguish between the carbon on the surface (which may be inactive) and the carbon in the iron phase (which may be active) can help resolve this controversy.

Many of the techniques that have been used to study iron catalysts, such as Mössbauer spectroscopy, XRD, and XPS, do not have the spatial resolution to provide information on catalyst microstructure. Since solid-state phase transformations (such as those from the iron oxide to the metal or the carbide) play a major role in determining catalyst activity, longevity, and atttrition, we have focused this study on the microstructure of these catalysts during the activation step. High resolution transmission electron microscopy (HRTEM) is unique in that it allows a study of the spatial distribution of various phases in the sample. For instance, HRTEM allows us to distinguish between magnetite formed during passivation of the catalyst versus the magnetite formed from hematite due to phase transformations that occur during activation. The combination of HRTEM with other bulk techniques like XRD, elemental analysis, and surface techniques such as XPS provides unique insights into the microstructural evolution of the catalyst. The results obtained in this study help to elucidate the nature of the active phase and the phenomena responsible for attrition and deactivation in iron catalysts.

EXPERIMENTAL

The catalyst used in this study was precipitated Fe_2O_3 obtained from the Department of Energy, Pittsburgh Energy Technology Center (PETC), United Catalysts Inc. #1185-78-370; L-3950 type. The catalyst was precipitated from a sulfate precursor, spray-dried, and calcined at 573 K. It was analyzed as 88.95% Fe_2O_3, 11% CuO, and 0.05% K_2O. CuO was added to lower the reduction temperature of Fe_2O_3 while K_2O served as a promoter for this low-α (low wax producing) FT catalyst.

For activity studies and preparation of TEM samples, Matheson research purity (99.99%) CO was used and further purified to remove carbonyls by passing through a column containing glass beads heated to 600 K, an ascarite column to remove CO_2, and a 7-μm Swagelok particle filter. H_2 and He were UHP (99.999%) obtained from Alphagaz and Argyle, respectively. The He was further purified by passing it through an AllTech Oxy-Trap. The O_2 used in passivation was of UHP (99.993%) purity obtained from Big. 3. The He used in the GC was Argyle 99.9% pure. The reactor was a differential fixed bed reactor consisting of a quartz U-tube with a bulb in which a known weight of catalyst (approximately 1 g) was placed over a quartz wool plug. The reactor was enclosed by an electri-

cally heated Griffin-Type Series-O heating mantle (750 W), and the catalyst temperature was monitored and controlled by a type K thermocouple connected to an Omega PID controller which maintained the temperature to within 2 K of the set temperature. The gas flow rates were set and controlled by Tylan FC-260 mass flow controllers and were maintained to within 1 sccm for helium and 0.1 sccm for the other gases.

In all the reactor studies, approximately 1 g of the as-received catalyst was loaded into the reactor. Different batches were activated under three different activation conditions: (i) CO (with 3% Ar as internal standard), 20.6 sccm, 543 K, 2 h; (ii) H_2, 20 sccm, 543 K, 2 h; and (iii) H_2/CO (with 3% Ar) = 3.5:5.2 sccm (FT synthesis reaction mixture with $H_2/CO = 0.7$), 523 K, 2 h. These conditions are based on temperatures and gases used by PETC to activate these catalysts for testing prior to a large-scale pilot plant run.

After activation, reactions were carried out over the catalyst samples in the same reactor tube at 523 K with $H_2/CO = 0.7$ and a total gas flow rate of 8.7 sccm (with Ar as internal standard) at a pressure of 630 Torr (normal atmospheric pressure in Albuquerque). Three sets of samples were made, one for each of the three activation conditions. Each set consisted of three samples, after activation, activation followed by FT reaction for 10 h, and activation followed by FT reaction for 45 h. Before switching the flowing gases from the activation mixture to the reaction mixture, the reactor was cooled to room temperature and extensively purged with helium. In the case of the syngas activation, the first 2 h of the reaction run were considered the activation step. Therefore, the activation in this case was at 523 K. Separate runs with syngas activation at 543 K were also carried out to explore the effect of activation temperature.

The samples were removed from the reactor after careful and highly controlled passivation. This involved purging with He at the reaction temperature, cooling the sample to room temperature, and exposing it to small amounts of O_2 in a stream of flowing He until a final oxygen content of 20% was reached. The completion of the passivation process was marked by the occurrence of a small exotherm (typically 2–3 K) in the catalyst bed and the subsequent return to room temperature. The sample was then removed and stored in a glass vial for further characterization tests. To assess the efficacy of the passivation step, we examined a catalyst that was reduced in H_2 at 673 K to transform it into metallic Fe. TEM images showed a thin film of magnetite after air exposure, which was no more than 1–2 nm thick. The room temperature grown magnetite was crystalline and therefore easy to distinguish from the amorphous carbon films that resulted from use of the catalyst in the FT environment.

The Fischer–Tropsch synthesis for production of hydrocarbons can be generically represented as

$$n\mathrm{CO} + \{(m + 2n)/2\}\mathrm{H_2} \rightarrow \mathrm{C}_n\mathrm{H}_m + n\mathrm{H_2O}, \quad [1]$$

where C_nH_m is a general representation for hydrocarbons—alkanes and alkenes. Though hydrocarbons are the primary products, it must be noted that small quantities of alcohols are also known to be synthesized.

FT synthesis is also accompanied by two side-reactions, namely the water–gas shift (WGS) and the Boudouard reactions. These can be represented as

$$\text{Water gas shift} \quad \mathrm{CO} + \mathrm{H_2O} \leftrightarrow \mathrm{CO_2} + \mathrm{H_2} \quad [2]$$

$$\text{Boudouard reaction} \quad 2\mathrm{CO} \rightarrow \mathrm{C} + \mathrm{CO_2}. \quad [3]$$

The occurrence and extent of these two reactions depends strongly on the nature of the catalyst and is especially rapid on iron catalysts. The extent of WGS is limited by the amount of water available and is thermodynamically favored at low temperatures (K_{eq} = 110 at 523 K) (17). In this case, almost all the water formed in FT synthesis is consumed in WGS and the oxygen from the reacting CO appears in the product stream as CO_2.

The product gases were analyzed in a Varian 3400 Gas Chromatograph (GC) and the peak areas were integrated by a Varian 4270 integrator. Analyses were done with a Thermal Conductivity Detector (TCD) with He as a reference gas for the detector. The CO feed stream had 3% Ar as an internal standard so that the conversion of CO could be directly measured. The column used was a 0.125-in × 15-ft stainless steel column with 80/100 Supelco Carboxen 1000 packing. The difference in the Ar/CO count ratio in the feed or bypass stream and during the reaction gave a measure of the conversion. Since CO_2 and CO were both detected by the TCD, we were able to monitor both the reduction of the catalyst (which yields one CO_2 per CO consumed) and the FT synthesis + water gas shift (0.5 mole CO_2 per mole CO consumed), and the Boudouard reaction (also 0.5 mole CO_2 per mole CO consumed).

Three parameters were used in order to deduce the influence of the activation treatment on the behavior of the catalyst. These were the rate of CO conversion and the rate of CH_4 formation, computed in micromoles/g raw catalyst-sec, and the percent CO_2 selectivity, representing the amount of CO_2 produced per mole of CO consumed.

The calculations were done as follows:

1. CO conversion. Fractional conversion (x):

$$x = \frac{[\mathrm{CO/Ar}]_{\mathrm{run}}}{[\mathrm{CO/Ar}]_{\mathrm{feed}}}. \quad [4]$$

$$\text{Rate}_{CO} = \mu\text{mol CO consumed/g raw catalyst} - \text{sec}$$

$$= \frac{[x] \times [\text{CO}]_{\text{feed(sccm)}} \times 10^6}{60 \times 22.4 \times 10^3 \times [\text{cat.wt.(g)}]}. \quad [5]$$

2. CH_4 formation.

$$\text{Rate}_{CH_4} = \mu\text{mol } CH_4 \text{ formed/g raw catalyst} - \text{sec}$$

$$= \frac{[\text{Rate}_{CO}] \times [CH_4/\text{Ar}]_{\text{run}}}{[\text{CO/Ar}]_{\text{feed}} \times [x]}. \quad [6]$$

3. CO_2 selectivity (percent).

$$\frac{100 \times [CO_2/\text{Ar}]_{\text{run}}}{[\text{CO/Ar}]_{\text{feed}} \times [x]}. \quad [7]$$

The counts of all the gases were corrected for TCD analysis by dividing the absolute counts obtained from the integrator by their molar response factors (18).

The catalyst microstructures were studied by both scanning and transmission electron microscopy using a Hitachi S-800 SEM, JEOL JEM 2000FX TEM (3.0 Å point resolution and a JEOL JEM 2010 TEM (1.9 Å point resolution). For the SEM, the sample was mounted on an Al stub while copper grids with holey carbon films were used for the TEM. The grids were dipped into the sample and the excess sample was shaken off. No solvents were used at any stage of the process to avoid hydrocarbon contamination.

Surface areas were measured by the BET method using a Micromeritics ASAP 2000 instrument. Carbon content of the catalyst samples was measured with a Perkin–Elmer 2400 CHN Elemental Analyzer. This analysis involves oxidizing the samples at 1000 K and measuring the amount of CO_2 formed. X-ray diffraction patterns were obtained with a Siemens D5000 Diffraktometer using 1.54 Å Cu K_α radiation. Powder X-ray diffraction patterns were obtained from all the samples in order to estimate the relative amounts of phases present. Since no internal standard was used in these experiments, the peak area serves only as a qualitative measure of the amount of each phase present.

All XPS and Auger electron spectroscopy (AES) experiments were performed in an ultra-high vacuum (UHV) chamber coupled to an atmospheric pressure reaction cell. This apparatus is identical to one described elsewhere (19) except that facilities for XPS and ion scattering spectroscopy (ISS) have been added. All XPS and AES results were obtained from samples treated *in situ* in the reaction cell and transferred into the UHV chamber without exposure to air. Detailed sample mounting procedures are described in Ref. (19). AES was performed using a Perkin–Elmer Model 15-155 cylindrical mirror analyzer, with excitation of the Auger process provided by a 3 keV, 4 μA, 100 μm diameter electron beam generated by a coaxial

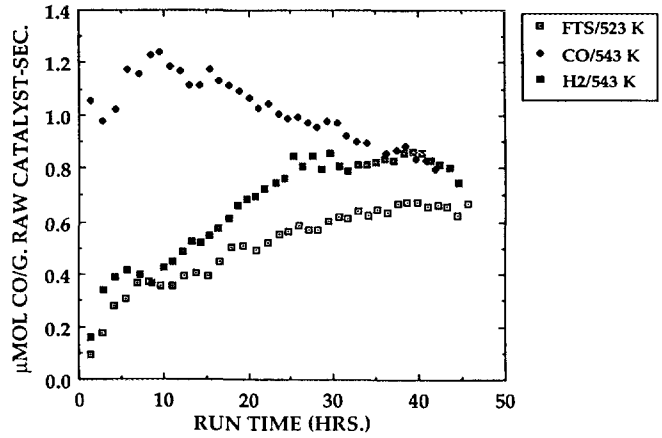

FIG. 1. CO consumption during Fischer–Tropsch synthesis as a function of time for the Fe_2O_3 catalyst activated in syngas at 523 K, CO at 543 K, and H_2 at 543 K for 2 h. Reaction temperature = 523 K, reactant ratio H_2O/CO = 0.7.

electron gun mounted within the analyzer. Details of data collection and manipulation are provided in Ref. (19). XPS was performed with a VG Microtech CLAM2 hemispherical analyzer operated at a pass energy of 50 eV and a slitwidth of 4 mm. A 600 W Al K_α X-ray source oriented 50° away from the analyzer lens axis provided primary excitation. Thermal gravimetric analysis (TGA) was performed on the samples in a TA Instruments Model 951 thermogravimetric analyzer connected to a TA Instruments Thermal Analyst 2000 data acquisition and control system. Three different gases were used, H_2 (99.999% H_2, Matheson), CO (99.99% CO, Matheson), and a H_2/CO synthesis gas mixture (47.2% H_2, 49.7% CO, 3.1% Ar, Matheson). The iron catalyst was heated at 5 K/min to 543 K in either H_2 or CO flowing at 60 sccm and then held at 543 K for 10–14 h in the flowing gas until the rate of weight change was negligible. The sample was cooled to room temperature and the gas was switched to the synthesis gas mixture flowing at 60 sccm. After flushing with reactant gas at room temperature for 3–5 min, the temperature was raised at 5 K/min to the reaction temperature. The weight gain of the sample was recorded for 14 h at the reaction temperature.

RESULTS

FT Synthesis Activity

The rate of CO conversion plotted in Fig. 1 includes the CO consumed due to reactions 1 and 2 as well as for catalyst reduction and carbidization. As can be seen from Fig. 1, the CO-activated sample shows the largest rate of CO conversion, which goes through a maximum and decreases after a few hours on stream. The highest activity in Fig. 1 corresponds to a conversion of 30%. Since the

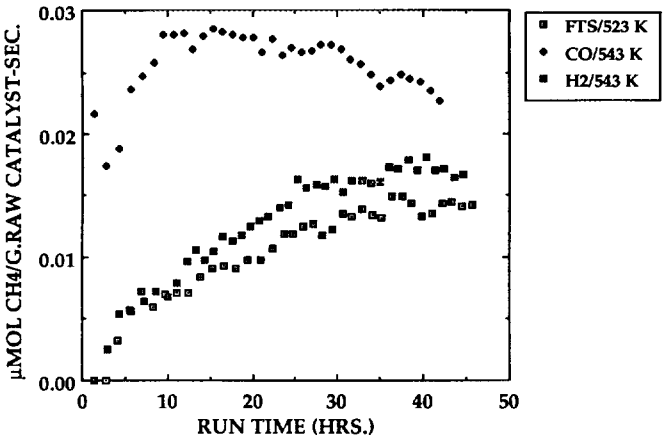

FIG. 2. CH_4 formation during Fischer–Tropsch synthesis as a function of time for the Fe_2O_3 catalyst activated in syngas at 523 K, CO at 543 K, and H_2 at 543 K for 2 h. Reaction temperature = 523 K, reactant ratio H_2/CO = 0.7.

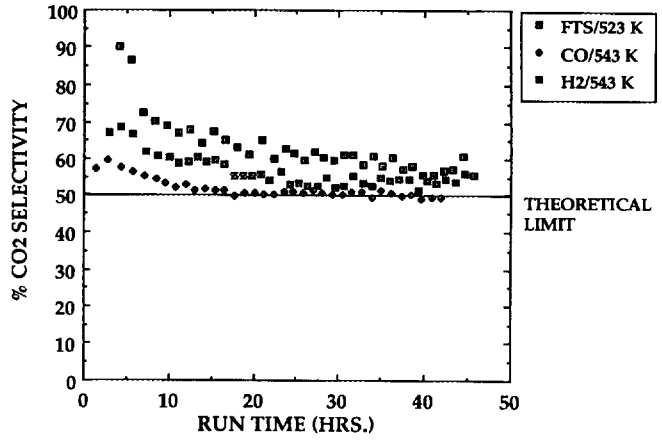

FIG. 3. CO_2 product selectivity during Fischer–Tropsch synthesis as a function of time for the Fe_2O_3 catalyst activated in syngas at 523 K, CO at 543 K, and H_2 at 543 K for 2 h. Reaction temperature = 523 K, reactant ratio H_2/CO = 0.7.

amount of catalyst used was identical for all three activation conditions, the actual conversion for all other runs can be obtained by scaling this value based on activity. The other two activation treatments show lower CO consumption activity which gradually increases over time. The maximum activity for the H_2 activated catalyst is 21% conversion at 39 h vs 17% conversion at 40 h for the synthesis gas activated sample. At the end of the run (40 h), the CO conversion rate for the H_2-activated sample is comparable to that of the CO-activated sample, while the rate of CO conversion for the sample activated in the FT reaction mixture is only slightly lower.

The activity trends are also reflected in the CH_4 formation plots (Fig. 2) indicating the FT activity of the various samples. It can be seen that the H_2- and FT-activated samples show no initial methane formation, while the CO-activated sample is initially active for FT synthesis. At the end of the run, the CH_4 formation rate on the CO-activated sample is still higher than that of the other two samples. The FT-activated sample has the lowest rate of CH_4 formation. We have not quantified any of the hydrocarbons other than CH_4 since our GC system was not set up for this purpose. We were able to detect C_2 and C_3 in small amounts, but the peaks were extremely broad under our experimental conditions. We also detected hydrocarbon oils when the catalysts was removed after reaction. These oils accumulated at the bottom of the quartz U-tube, but were not quantified. The CH_4 formation rate is therefore the only indicator of FT activity of this catalyst.

From the stoichiometry of the FT synthesis and its associated reactions (Eqs. [1]–[3]), it can be seen that if the WGS reaction reaches equilibrium (K_{eq} = 110) at 523 K (17), a maximum CO_2 selectivity of 50% is achieved. Under these conditions, the excess CO_2 selectivities above 50% imply CO_2 formed by reduction of the catalyst. The CO_2 selectivity (Fig. 3) therefore serves as a measure of catalyst reduction during the run. From Fig. 3, it can be seen that the CO-activated sample does not undergo further reduction, while the other two samples continue to get reduced over the entire length of the run.

CHN Analysis

Table 1 shows the results of CHN analysis used to determine the weight percent carbon as a function of activation and reaction. The CO-activated sample had a higher carbon content after the activation treatment than the other two samples, which contained negligible amounts of carbon after activation. Over the course of the reaction, the carbon content of the CO-activated sample was consistently higher than the other samples. The sample activated in the FT reaction mixture had the lowest carbon content at any point in the run. For comparison with the measured carbon contents, the calculated carbon content in each carbide phase is 6.7% in Fe_3C, 7.9% in χ-$Fe_{2.5}C$, 8.9% in ε'-$Fe_{2.2}C$, and 9.7% in ε-Fe_2C.

TABLE 1

Carbon Content (wt%) of the Catalyst Measured by the CHN Analyzer after Activation and Reaction

Treatment	Activation	Activation + reaction for 10 h	Activation + reaction for 45 h
H_2/543 K	0	1.9	6.2
CO/543 K	3.1	6.9	10.6
Syngas/523 K	0.2	1.6	5.1

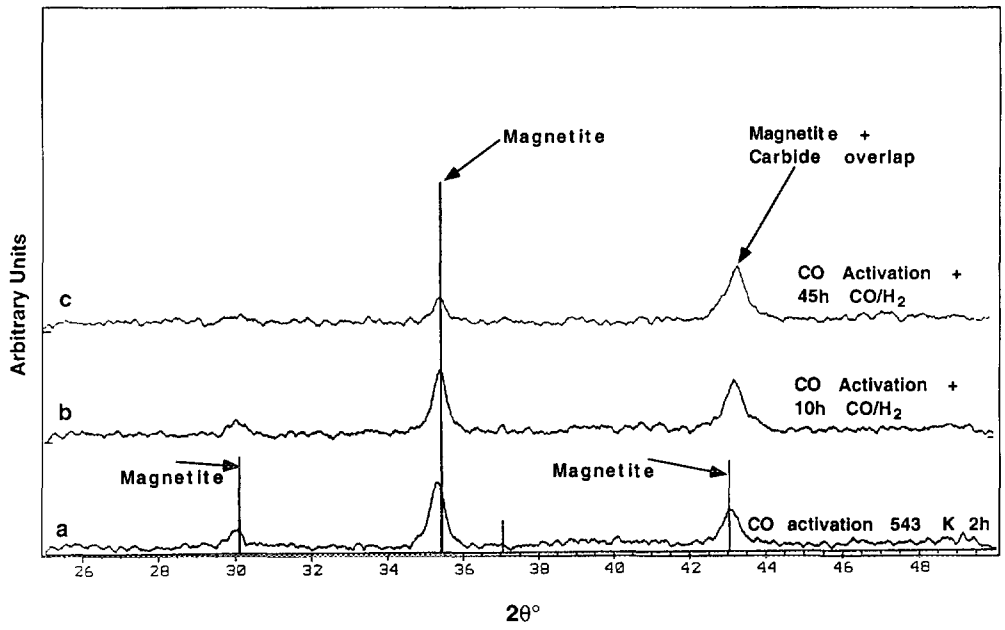

FIG. 4. XRD spectra of the Fe_2O_3 catalyst after (a) activation in CO for 2 h at 543 K, (b) activation in CO followed by Fischer–Tropsch synthesis for 10 h at 523 K, and (c) activation in CO followed by Fischer–Tropsch synthesis for 45 h at 523 K.

XRD Analysis

X-ray powder diffraction patterns of the CO-activated sample after activation, and after 10 and 45 h of FT synthesis are shown in Fig. 4. The pattern has been plotted over 2θ values ranging from 25° to 50° since the most intense peaks of the magnetite as well as the carbide phase happen to fall over this range of angles. The pattern in Fig. 4a shows that after activation, prominent magnetite peaks are seen at 2θ values of 30°, 35.5°, and 43°. After syngas exposure for 10 h at 523 K, the XRD spectrum changes only slightly, but a pronounced change is seen in the sample exposed to syngas for 45 h at 523 K. In Fig. 4c, the magnetite peaks (at 30° and 35.5°) have greatly diminished in intensity while the peak at ~43° remains relatively unchanged. Since most of the carbide phases reported in the JCPDS (20) database have prominent peaks around 2 Å, we have assigned the peak at ~43° to the carbide phase. Since the peak is broad, it is not possible to specify which carbide we have obtained under these conditions. We have therefore referred to the carbide in this work as Fe_xC since we do not know the stoichiometry. Since TEM shows that the carbide is invariably covered with carbon layers, we also cannot determine the stoichiometry from bulk elemental analysis.

From Fig. 4, it can be seen that the carbide peak at around 43° overlaps with the magnetite peak at the same 2θ value. Since we did not use an internal standard, direct quantification of the amounts of various phases present was not possible. We have therefore used the peak area for most intense reflection for each phase as a qualitative measure of the amount of that phase. Table 2 shows the ratio of the peak at 35.5° (the most intense magnetite peak) with the 43° peak (most intense carbide peak overlapping with the 30% intensity magnetite peak). Also shown in Table 2 is an estimate of the percentage of carbide in the sample obtained by using the ratio of the 35.5° and 43° peaks. If this ratio is 3.33, the sample contains 100% magnetite, with the ratio going to 0.0 when the magnetite transforms completely to carbide. This analysis ignores other

TABLE 2

Analysis of XRD Patterns

Treatment	Ratio of XRD peak at 35.5° to that at 43°	Carbide × 100 / (Carbide + Magnetite)
CO activation, 543 K, 2 h	2.12	36.0
Activation + 10 h, CO/H_2	0.99	70.1
Activation + 45 h, CO/H_2	0.29	91.2
H_2 activation, 543 K, 2 h	3.51[a]	0.0
Activation + 10 h, CO/H_2	2.65	20.2
Activation + 45 h, CO/H_2	1.06	68.0
CO/H_2 activation, 523 K, 2 h	3.33	0.0
Activation + 10 h, CO/H_2	2.43	26.8
Activation + 45 h, CO/H_2	1.21	63.4

[a] Assumed to be 3.33 (the ratio for magnetite from JCPDS) since the sample contains magnetite as the only detectable crystalline phase.

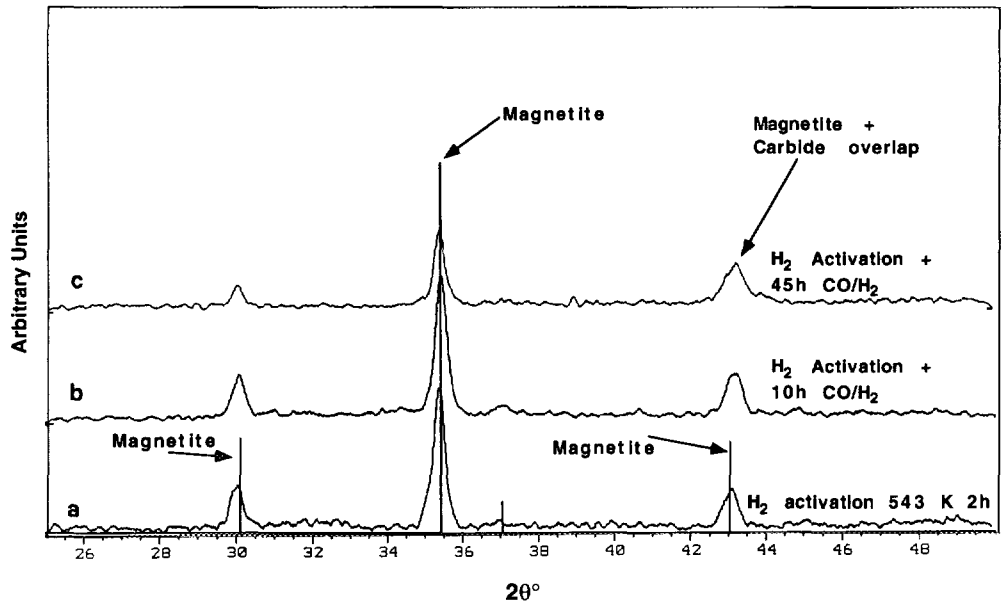

FIG. 5. XRD spectra of the Fe_2O_3 catalyst after (a) activation in H_2 for 2 h at 543 K, (b) activation in H_2 followed by Fischer–Tropsch synthesis for 10 h at 523 K, and (c) activation in H_2 followed by Fischer–Tropsch synthesis for 45 h at 523 K.

X-ray amorphous phases that may be present in the sample; no other crystalline phases other than carbide and magnetite were seen after activation.

Figures 5 and 6 show the corresponding XRD patterns for the H_2 and syngas activated samples. Both figures show that the sample transforms into magnetite after the initial activation, and even after 45 h of exposure to syngas, there is still some magnetite present. The XRD results are consistent with the CHN analysis showing that the greatest degree of carbon buildup occurs with the CO activated sample.

TGA Analysis

Thermal gravimetric analysis of the catalyst activated in CO was explored. The sample pretreated in CO decreased

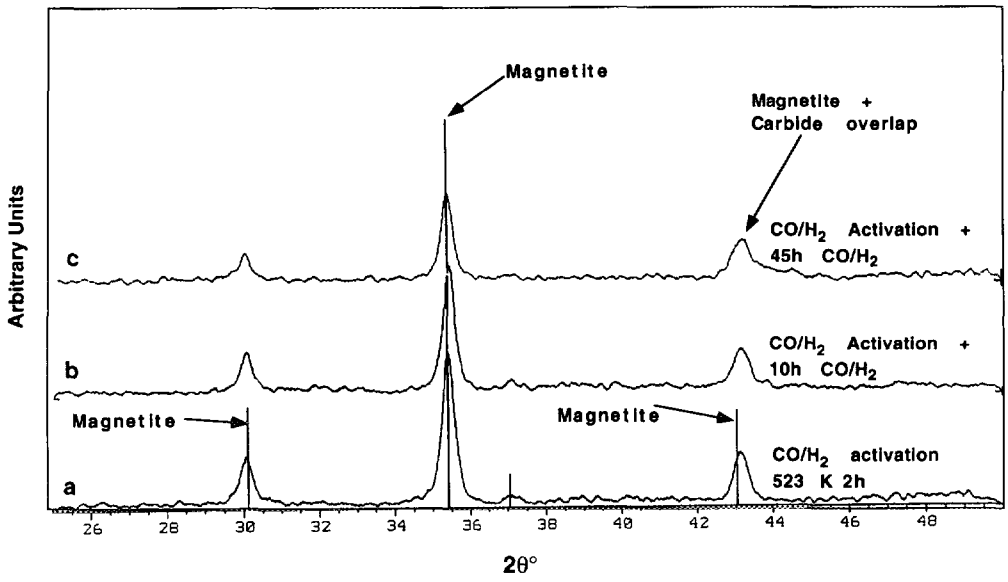

FIG. 6. XRD spectra of the Fe_2O_3 catalyst after (a) activation in H_2/CO (ratio 0.7) for 2 h at 523 K, (b) activation in CO/H_2 followed by Fischer–Tropsch synthesis for 10 h at 523 K, and (c) activation in H_2/CO followed by Fischer–Tropsch synthesis for 45 h at 523 K.

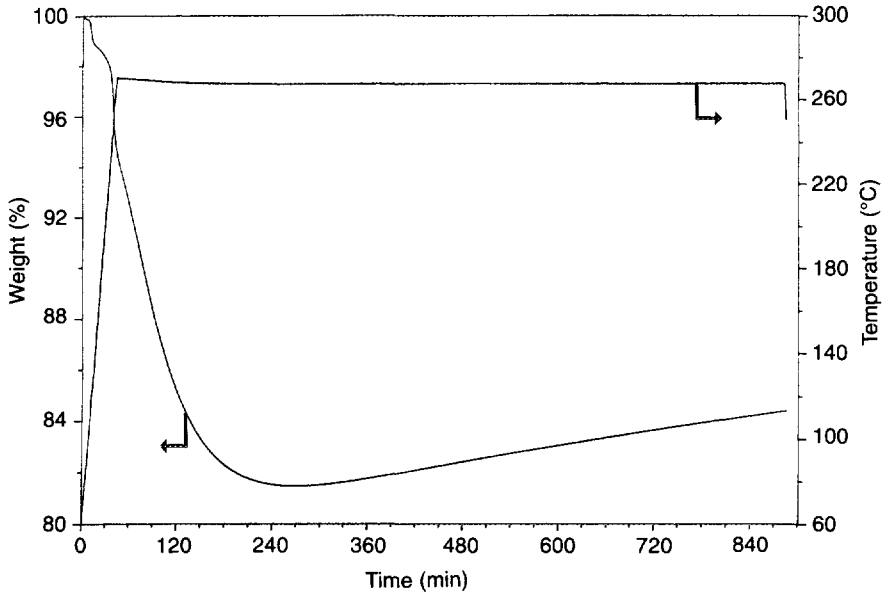

FIG. 7. Percent weight change measured by TGA as a function of time for the Fe_2O_3 catalyst exposed to CO at 543 K. Also shown is the temperature ramping sequence. Weight of the catalyst = 155.48; flow rate, 60 sccm CO.

to 82% of its original weight, as seen in Fig. 7, followed by a gradual increase in weight. The weight loss for transformation from hematite to magnetite is about 3.4%. This implies that a significant amount of carbide formation has occurred. (Hematite to Fe_3C reflects a 75% decrease in weight.) After cooling in CO, the sample was flushed with syngas at room temperature for 5 min and the temperature was ramped at 5 K/min to 523 K. There was a small weight loss of 1% followed by a gradual weight increase of 0.16% per hour (Fig. 8). The initial 1% weight decrease may correspond to the desorption of surface species formed on the catalyst during the 5-min flow of synthesis gas at room temperature prior to heating.

Similar experiments were performed by carrying out the

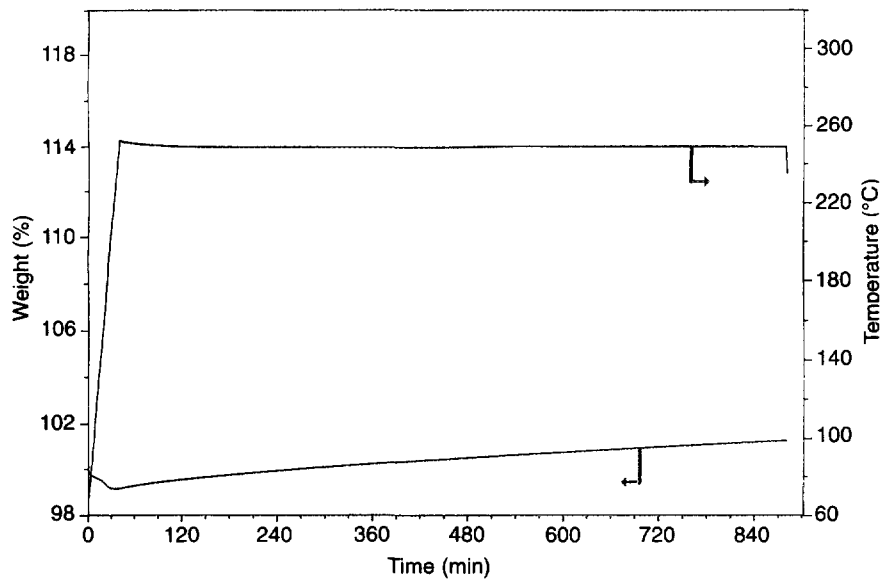

FIG. 8. Percent weight change measured by TGA as a function of time for the Fe_2O_3 catalyst exposed to syngas at 523 K following the activation in CO for 14 h shown in Fig. 7. Also shown is the temperature ramping sequence. Weight of the catalyst = 130.93 mg; Flow rate, 60 sccm CO/H_2 (ratio 1.05).

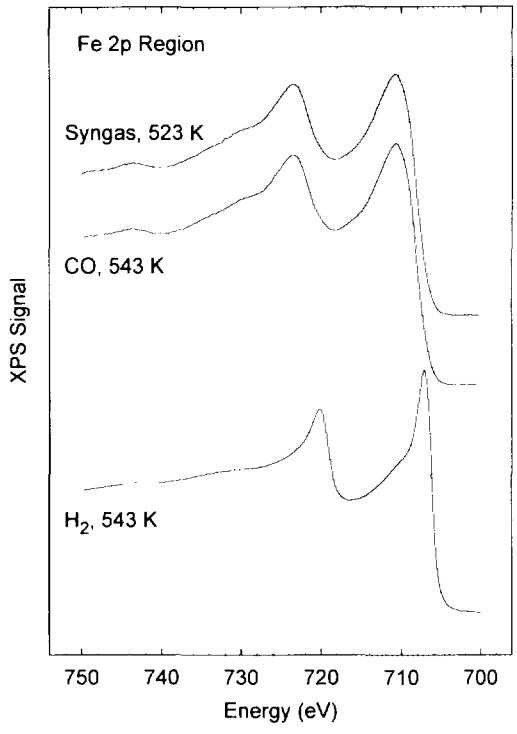

FIG. 9. X-ray photoelectron spectroscopy (XPS) results for the Fe_2O_3 catalyst activated in syngas at 523 K, CO at 543 K, and H_2 at 543 K for 2 h.

reaction at 548 and 573 K. The percent weight gain at these temperatures after the initial weight changes had occurred were 0.54% and 1.4% per hour, respectively. This weight increase implies significant carbon deposition on the surface of the catalyst since the only other possible reaction, bulk carbidization, would cause the sample weight to decrease as it goes from magnetite to iron carbide.

Surface Analysis

For the freshly calcined sample, XPS detects Fe_2O_3 as the sole iron phase present. In addition, copper, potassium, and small amounts of magnesium are observed on the catalyst surface. Since we are unaware of any intentional addition of Mg to the catalyst, it must be assumed that the Mg arises from minor impurities introduced during catalyst synthesis. XPS (Fig. 9) and AES (Fig. 10) spectra were also taken after each activation treatment. After both CO and syngas activation treatments, a single Fe $2p_{3/2}$ XPS peak is observed at a binding energy of 710.8 eV. The position of this peak, coupled with the absence of any shakeup features between 715 and 720 eV, unambiguously identifies magnetite as the primary phase detected in both cases (21). No evidence is seen for metallic iron or iron carbide phases, which would appear near 707 eV (21), or carbidic carbon, which would appear at ~283 eV (21).

While the XPS result for syngas activation is in complete agreement with XRD and TEM (see below), the absence of any carbide following CO activation is surprising given that XRD and TEM detect small amounts of carbide and TGA measures a significant amount of carbide under similar activation conditions. Based on past measurements of mixed iron carbide/oxide phases with this instrument, carbide levels as low as 4–5% should be detectable, leading to the conclusion that no more than 2–3% of the total surface iron detected is present as carbide following CO activation at 543 K for 2 h. AES supports the XPS analysis, showing a two-peak structure in the Fe(MVV) region between 40 and 55 eV, characteristic of iron oxides (22). Furthermore, the O(511 eV)/Fe(703 eV) ratios are lower than expected for Fe_2O_3, and the relative sizes of the three Fe(LMM) peaks at 598, 651, and 703 eV are intermediate between those of Fe_2O_3 and metallic iron (22). Taken together, this information supports assignment of the Auger spectra for the CO and syngas activated samples to magnetite.

In order to assess the ability of XPS to detect iron carbide in these catalysts, a sample of the catalyst after hydrogen activation and FT synthesis for 45 h was analyzed by XPS. Even though XRD (Table 2) and TEM (later in this paper) show that more than half the iron in this sample is carbided, XPS detects no carbide whatsoever. TEM shows that the

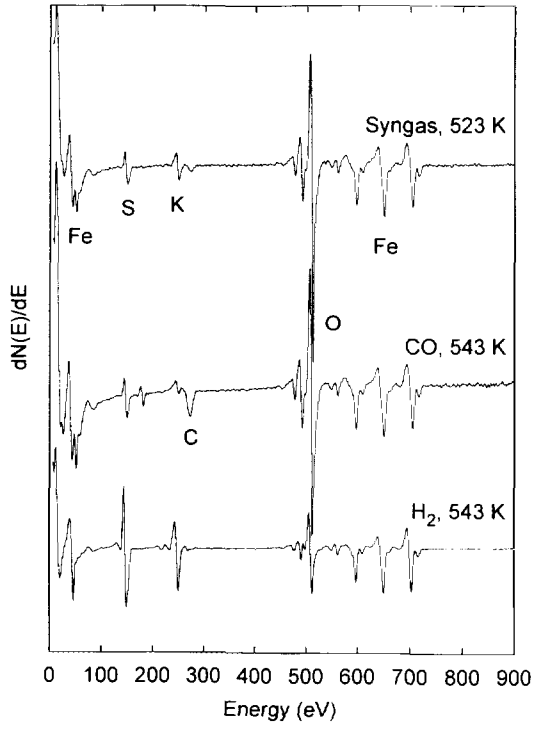

FIG. 10. Auger electron spectroscopy (AES) results for the Fe_2O_3 catalyst activated in syngas at 523 K, CO at 543 K, and H_2 at 543 K for 2 h.

carbide particles are covered by 3–4 nm amorphous carbon films, which undoubtedly attenuate the Fe $2p$ carbide signal and prevent its detection in the presence of magnetite. In support of this argument are the results of a depth profiling experiment in which the sample was bombarded with 5 kV Ar^+ ions at a current density of 1 $\mu A/cm^2$ for 1 h. Following this treatment, shoulders appeared in both the Fe $2p$ and C $1s$ regions at energies of 707 eV and 3 eV, respectively, much as observed by Reymond *et al.* (6). This result is a clear indication of the presence of carbide buried beneath a second phase. We will return to this aspect later in the discussion section.

XPS and AES detect small amounts of carbon on both the CO- and syngas-activated samples, with C $1s$ binding energies and C(272 eV) Auger peak shapes characteristic of graphitic carbon (23). While Fig. 10 shows a large carbon signal for the CO activated sample than for the syngas activated sample, this result was not reproducible, possibly due to the uncertainties in sample temperature measurements discussed in Ref. (19). It is clear, however, that carbon levels increase with activation time for both treatments. Although no carbidic carbon is seen by either XPS or AES, it is probable that graphitic overlayers on the carbide phase severely attenuate the carbide signals, as described above for attenuation of the Fe $2p$ carbide signal, and thereby prevent their detection.

XPS and AES of the hydrogen-activated sample show nearly complete reduction to metallic iron. The Fe $2p_{3/2}$ binding energy of 707 eV, and the single Fe(MVV) Auger peak at 47 eV are clear indicators of metallic iron. A small shoulder at ~710 eV on the Fe $2p_{3/2}$ peak and subtle differences between the Fe(MVV) lineshape of the activated sample and that of metallic iron (22) indicate the presence of some residual oxide. Note that the presence of a relatively large O(511 eV) peak cannot be taken as a direct indicator of iron oxidation since a fraction of the oxygen is associated with potassium (22). Detailed Fe(MVV) lineshape analysis (22) suggests that 35 to 45% of the O(511 eV) signal is due to iron oxides while the remainder is associated with potassium. The observation of nearly complete iron reduction by XPS and AES contrasts with XRD and TEM (see below), which show only magnetite following hydrogen activation. The disagreement can be reconciled by considering differences in the hydrogen activation conditions for the various techniques. In the case of AES and XPS, very small (~30 mg) samples were activated in batch conditions with a total hydrogen volume of ~500 cm^3, while for XRD and TEM, 1-g samples were activated in flowing hydrogen at a relatively low space velocity, and the possibility that a high partial pressure of water is present cannot be ignored. Complete reduction to metallic iron does occur in the flow reactor with more severe conditions. Following complete reduction, the catalyst surface area decreases from an initial surface area of 27 m^2/g to ~5 m^2/g.

In addition to demonstrating iron reduction during hydrogen activation, the XPS and AES results also show the appearance of large amounts of sulfur on the surface and growth of the potassium signal relative to iron. The growth of the potassium signal is attributed to the loss of surface area during reduction, which increases the potassium coverage. The appearance of sulfur is attributed to migration of sulfate impurities in the catalyst to the catalyst surface (19). Rough quantitative analysis (24) shows that the observed S(152 eV)/Fe(703 eV) ratio corresponds to approximately one monolayer of sulfur. Since sulfur is a well known poison for FT synthesis, this result suggests that complete reduction of this catalyst in hydrogen would result in little or no FT synthesis activity. This prediction is in agreement with our reactivity studies where reduction of the catalyst at 543 K for a week with 35 sccm of H_2 or at 723 K with 20 sccm of H_2 for 15 h resulted in a catalyst that was completely inactive for FT synthesis.

Scanning Electron Microscopy

SEM studies of the catalyst show the catalyst to be composed of spherical particles 20–70 μm in diameter with a fair amount of fines that may have broken off from the spherical particles. These fines all reduce in size, even the primary particles which are single crystals of α-Fe_2O_3 as explained below. The SEM images are consistent with particle size distributions obtained from a Micromeritics Sedigraph 5100 which show a bimodal distribution with peaks at 30 and 0.9 μm (25). The spherical agglomerates (Fig. 11a) are composed of smaller plate-like crystals which are angular and faceted as seen in Fig. 11b. Samples after activation or reaction show a higher proportion of fines and some extent of breakage at these length scales. Figure 12 shows an SEM image of a sample activated in CO at 543 K and subjected to FT synthesis at 523 K for 45 h. We observed a much rougher surface of the spheres with filament/tendril-like outgrowths which might shear off during the reaction in the slurry reactor. The broken particle suggests fracture during activation and subsequent reaction. To obtain a better understanding of the morphological changes in these catalysts, we also determined the BET surface areas, shown in Table 3.

Transmission Electron Microscopy

Figure 13 shows a typical image of the primary particles that make up the spherical agglomerates shown in Fig. 11. These particles are single crystals of α-Fe_2O_3 as confirmed by electron diffraction (25). These single crystals have a characteristic contrast consistent with the presence of voids within the single crystal matrix. The circular features exhibit a characteristic light/dark contrast with changes in

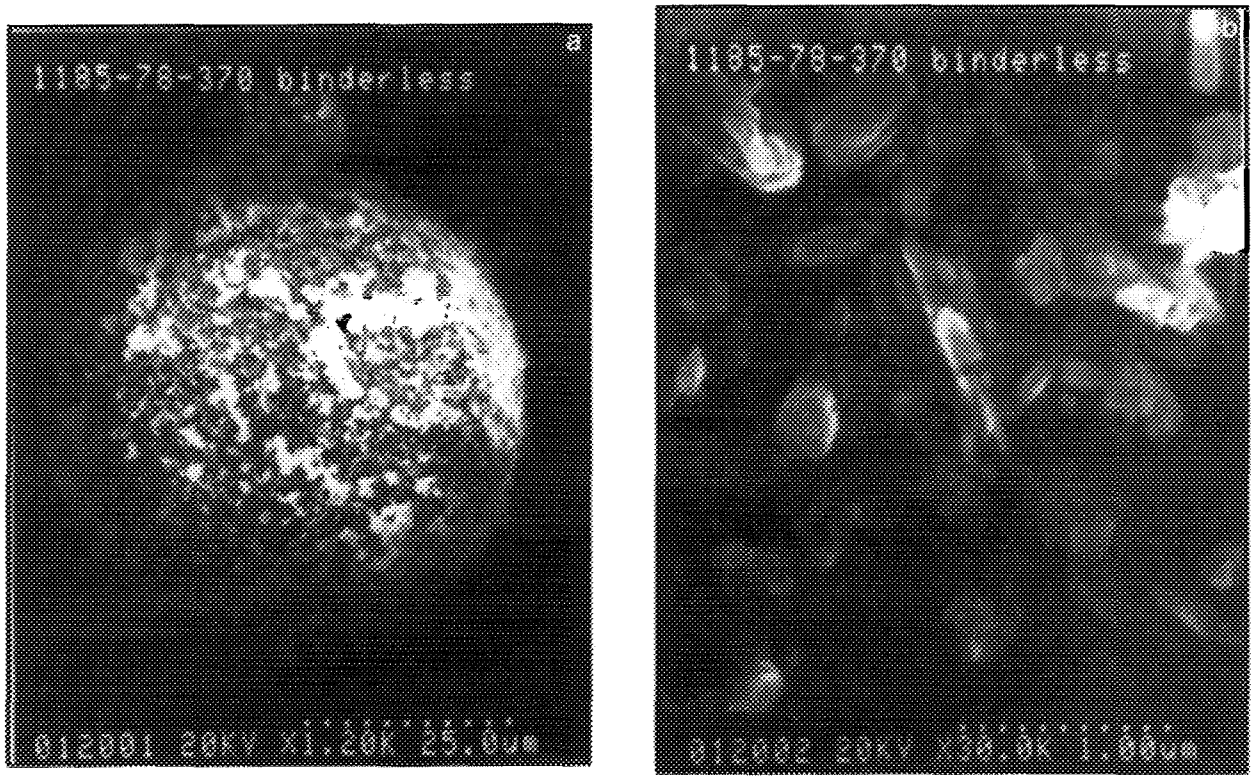

FIG. 11. SEM micrographs of the as-received catalyst. (a) Low magnification view showing the size and shape of the agglomerate and (b) high magnification view showing the angular nature of the particles forming the agglomerate.

focus, which is typical of voids. These voids do not disrupt the crystal structure since the lattice fringes go through them. In subsequent discussions, we refer to this microstructure as the "swiss cheese" morphology.

Sample Microstructure after Activation

Activation of 1 g of catalyst using 20 sccm of H_2 at 543 K transforms the sample into magnetite, as shown in Fig. 14a as well as the XRD pattern in Fig. 5a. As mentioned above, with more severe reduction treatment, we were able to obtain metallic iron, which is consistent with the XPS spectrum shown in Fig. 9. Complete reduction could be achieved by increased H_2 space velocity, higher temperatures, or longer reduction times. For example, as seen in Fig. 14b, activation for 15 h at 723 K of 1 g of catalyst transformed the sample to α-Fe, as confirmed by XRD and electron diffraction. A thin film of oxide formed on the surface of the sample during the controlled passivation in the reactor. Electron diffraction showed a faint ring indicating the presence of polycrystalline magnetite. This oxide film was different in appearance from the magnetite resulting from the phase transformation of hematite which retained the swiss cheese morphology. Furthermore, the crystallinity of the film helped to distinguish it from the amorphous and graphitic carbon that forms during exposure to syngas or to CO. Although complete reduction to the metal was possible, for subsequent reactivity studies we used the mildly reduced sample which had transformed into magnetite, since the fully reduced sample is inactive for FT synthesis due to sulfur poisoning.

In contrast to the H_2 activation, a 2-h CO activation of 1 g of catalyst with 20 sccm of CO at 543 K transformed the α-Fe_2O_3 into Fe_3O_4 plus small amounts of carbide (Fig. 14c). The presence of the carbide was deduced from electron diffraction and is consistent with the results from XRD and CHN analysis. We find that the carbide is always covered with a surface film, which we attribute to amorphous carbon. Activation in the syngas mixture for 2 h at 523 K shows no carbide but only magnetite (Fig. 14d). In these images, the presence of magnetite is seen by electron diffraction as well as by the presence of regions with remnants of the swiss cheese morphology of the original hematite catalyst.

Sample Microstructure after Activation and 10-h Reaction

After a short reaction period, sample morphologies are quite different (Fig. 15). The H_2-activated sample shows some extent of carbide formation, although most of the

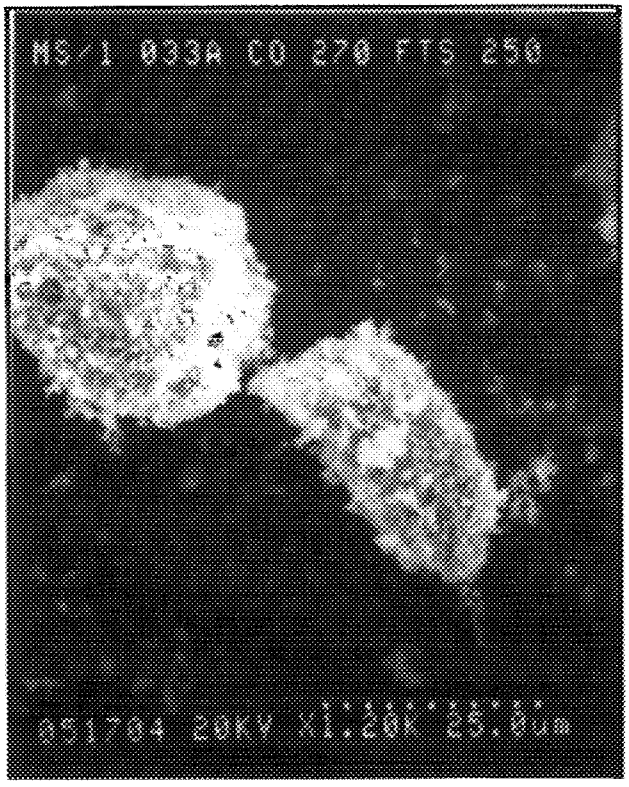

FIG. 12. SEM image of the Fe_2O_3 catalyst after activation in CO at 543 K for 2 h followed by FT synthesis at 523 K for 45 h.

sample is still magnetite. The carbide particles grow out of the magnetite as nodules on the surface (for example, Fig. 15a). This phase transformation starts to break up the initial single-crystal swiss cheese morphology by outgrowth of the carbide phase. The CO-activated sample (Fig. 15b) shows a much greater degree of transformation into carbide, while the syngas-activated sample (Fig. 15c) shows a smaller extent of carbide formation. The carbide particles are invariably covered by a surface film, similar to that seen in Fig. 14c, while the magnetite surface is clean. We attribute these surface films to amorphous carbon formed during reaction.

TABLE 3

BET Surface Area (m^2/g) Measured after Activation and Reaction (Surface Area of As-Received Catalyst = 27 m^2/g)

Treatment	Activation	Activation + reaction for 10 h	Activation + reaction for 45 h
H_2/543 K	20.7	23.6	20.7
CO/543 K	44.2	33.6	23.2
FTS/523 K	31.8	28.3	24.4

Sample Microstructure after Activation and 45-h Reaction

After a 45-h reaction, all samples show significant amounts of carbide formation, although the H_2-(Fig. 16a) and FT-(Fig. 16b) activated samples still have some magnetite present. The CO-activated sample (Fig. 16c) shows very small traces of magnetite. A common feature in all samples, irrespective of the nature of the activation treatments or the extent of the reaction, is the occurrence of 3–4 nm thick films of amorphous carbon only on the carbide particles. The magnetite phase, where present, is not covered by any overlayers. With electron and X-ray diffraction, it is not possible to distinguish between the various carbide phases since they all had primary diffraction peaks extremely close to each other. The major peak from the carbide formed in our samples is a broad reflection centered around a 2θ value of 43°. In the TEM images, carbide grains appear as small crystallites showing d spacings of ~2 Å. For this reason, we have chosen to label the carbide phase as a single iron carbide without reference to its precise stoichiometry.

DISCUSSION

The Role of Activation

When precipitated, unsupported iron oxide catalysts are exposed to FT synthesis reaction environments, the catalysts transform from hematite into one or more carbides, regardless of the activation step. The activation process controls the rate of the transformations. These processes are schematically illustrated in Figs. 17 and 18. As shown in Fig. 17, the single crystals of hematite first transform into magnetite retaining the characteristic swiss cheese morphology. This step is relatively facile and is complete within 2 h for all activation treatments. In another study (25), we show that this transformation can occur at lower temperatures. The subsequent transformation from magnetite to carbide is slow and depends on the activation environment. The carbide phase forms as small nodules on the surface of the magnetite with the phase transformation proceeding slowly into the bulk. The breakdown of the original single crystals is brought about by this phase transformation. Figure 18 summarizes the differences in the extent of transformation caused by the different activation treatments. The horizontal bars in Fig. 18 are divided into three segments to show the three significant transformation steps: (1) hematite to magnetite, (2) nucleation of the carbide, and (3) nearly complete transformation into carbide.

Based on the rate of CH_4 formation, which we consider to be an indicator of FT activity, we find the CO activation to be the most effective method for activating the catalyst. Similar conclusions are obtained if weight gain per unit time is used as a measure of FT activity. Activation in CO transforms the hematite into magnetite and small amounts

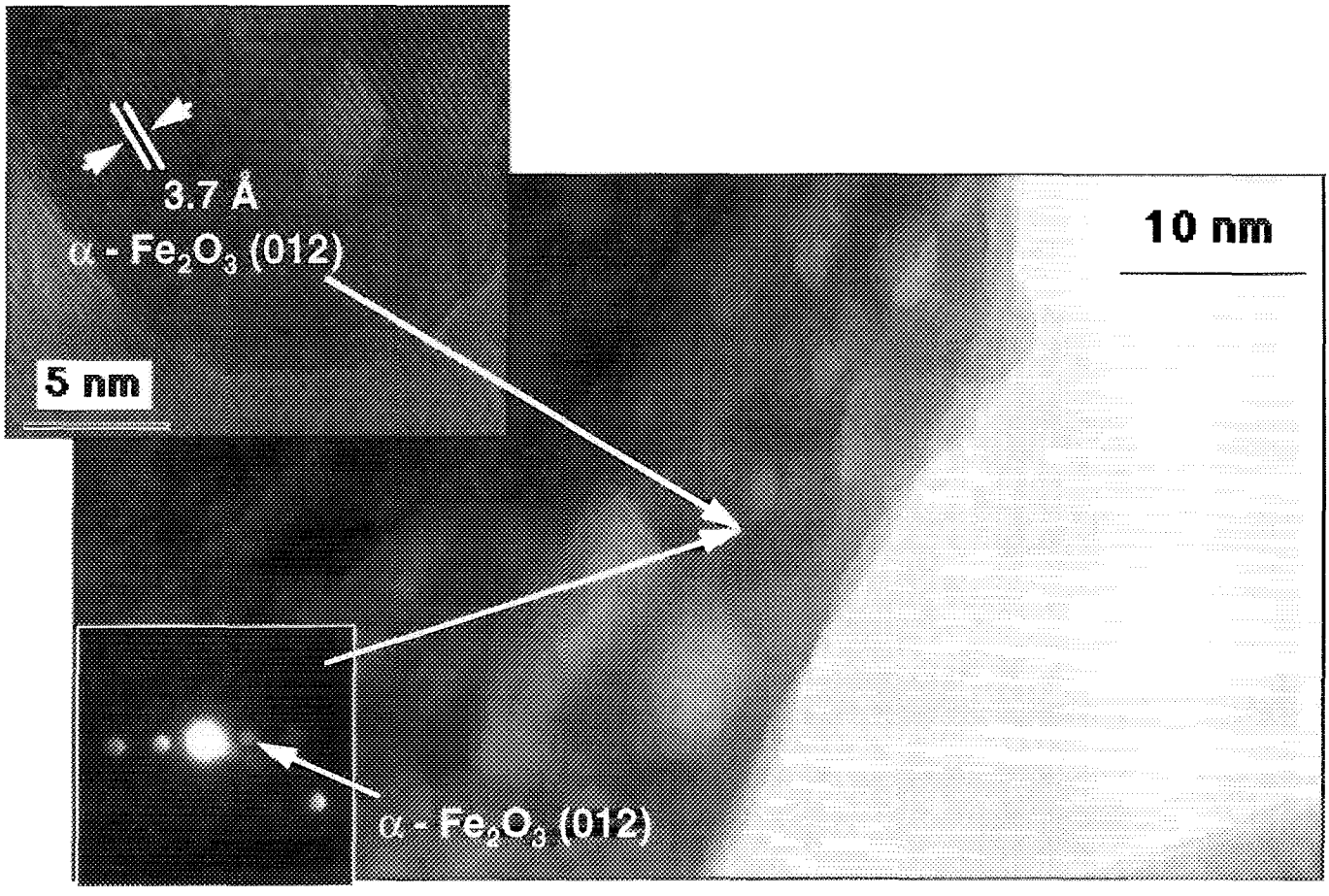

FIG. 13. TEM view of the primary particles that make up the agglomerate shown in Fig. 11a. Electron diffraction (inset) shows these particles to be single crystals of α-Fe_2O_3.

of carbide at the end of the 2-h activation step. With H_2 activation under mild reduction conditions, we see only magnetite and the catalyst shows no initial FT activity, although some CO_2 is formed. The behavior with syngas activation is similar to that observed for H_2 activation. The syngas mixture may have been unable to transform the sample into carbide during the 2-h activation period since the activation was performed at the reaction temperature 523 K instead of the 543 K used for the CO-activated procedure. When syngas activation was performed at 543 K, we did see evidence of initial FT activity and the presence of carbide. However, the subsequent activity as a function of time is very similar to that of the sample activated at 523 K.

The activation process is profoundly affected by the space velocity of the activation gases. For instance, CO activation in the TGA (60 sccm, 150 mg of catalyst) results in a much greater extent of carbide formation than in the fixed-bed reactor (20 sccm, 1 g of catalyst). With H_2, higher space velocities result in complete reduction to metallic iron; however, complete reduction causes migration of sulfur impurities to the catalyst surface as seen by XPS and AES. Complete reduction to metallic iron yields a catalyst that cannot be easily carbided and has no FT activity, although some CO_2 is formed. In the flow reactor experiments, where the low H_2 flow rates cause a mild reduction transforming the hematite to magnetite but not to the metal, the catalyst can be carbided and does develop FT activity in the syngas mixture.

These transformations involve a major breakdown of the single crystal hematite particles into smaller crystallites of carbide, but there is no corresponding increase in the BET surface area, as seen in Table 3. The surface area after reaction remains at ~27 m^2/g (the surface area of the as-received catalyst). The hematite crystals are platelets about 1 μm long, 0.3 μm wide, and approximately 40–50 nm thick. The surface area can be calculated as follows:

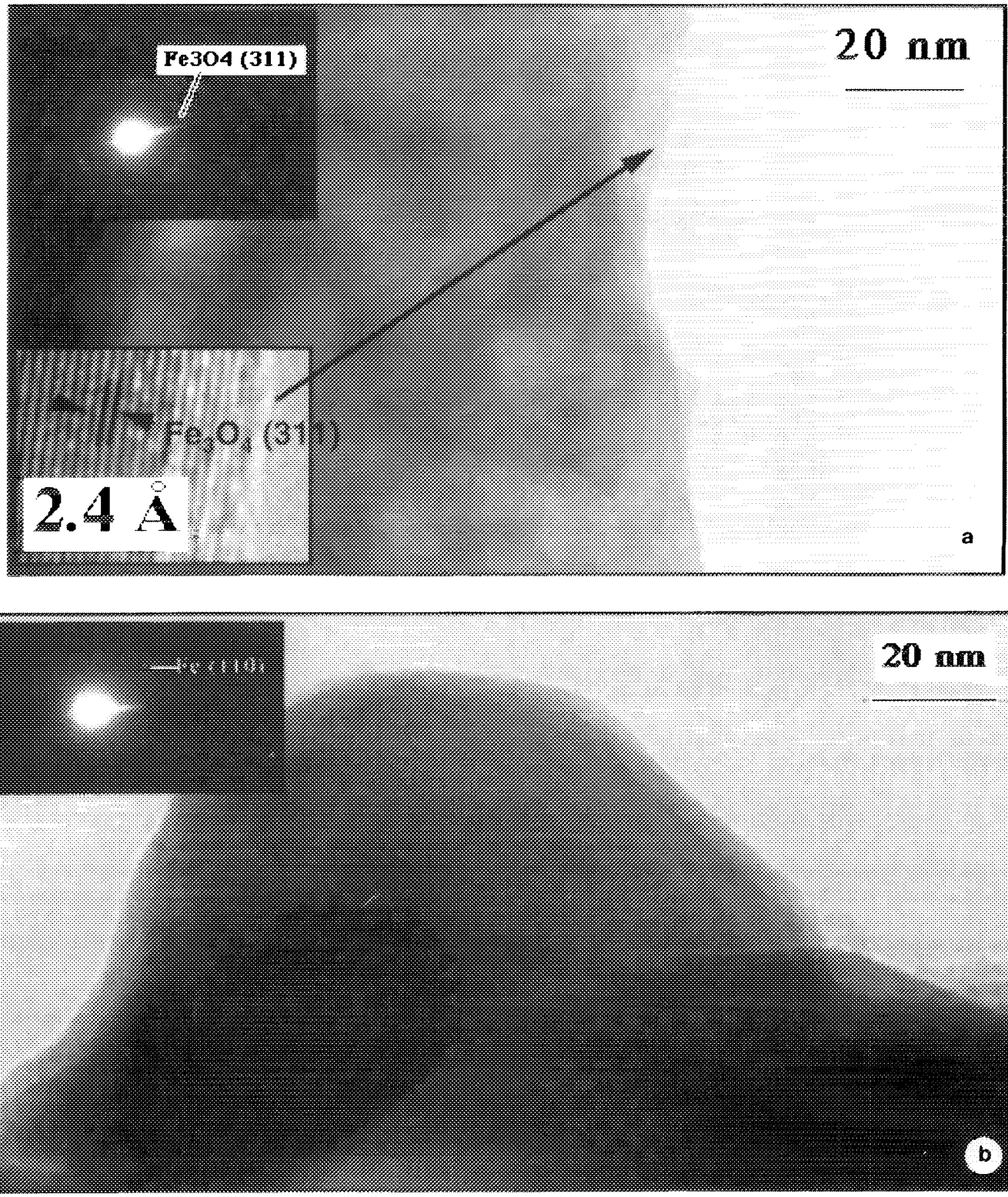

FIG. 14. TEM view of the α-Fe_2O_3 catalyst after activation treatments. (a) After activation in H_2 at 543 K for 2 h. Electron diffraction (inset) shows the catalyst to have transformed into magnetite (Fe_3O_4). (b) After exposure to H_2 at 723 K for 15 h. Electron diffraction (inset) shows the catalyst to have undergone complete reduction to form α-Fe. (c) After activation in CO at 543 K for 2 h. Electron diffraction (inset) shows the catalyst to have transformed into magnetite (Fe_3O_4). Also seen are small amounts of Fe carbide. (d) After activation in syngas mixture (H_2/CO = 0.7) at 523 K for 2 h. Electron diffraction (inset) shows the catalyst to have transformed into magnetite (Fe_3O_4).

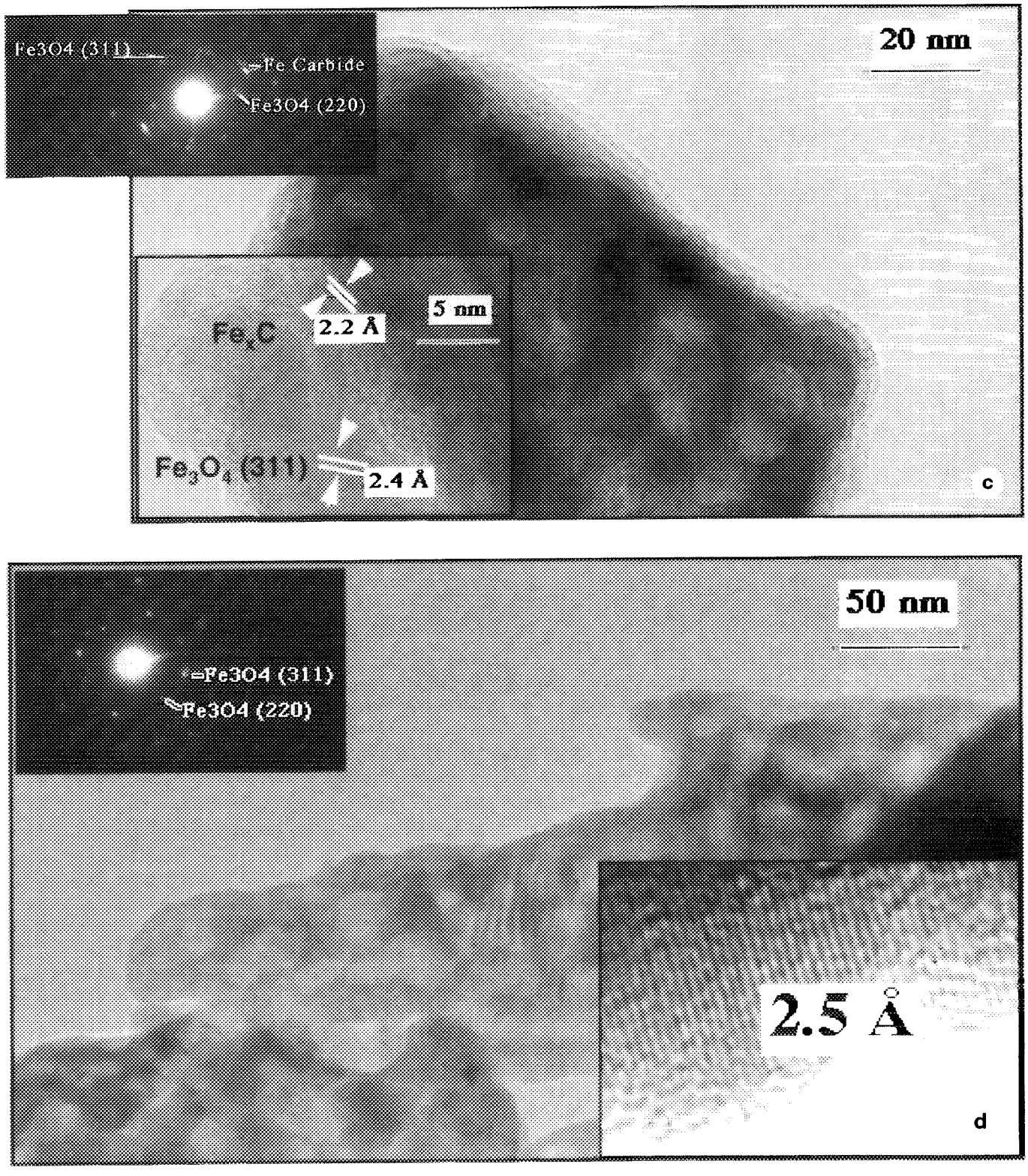

FIG. 14—*Continued*

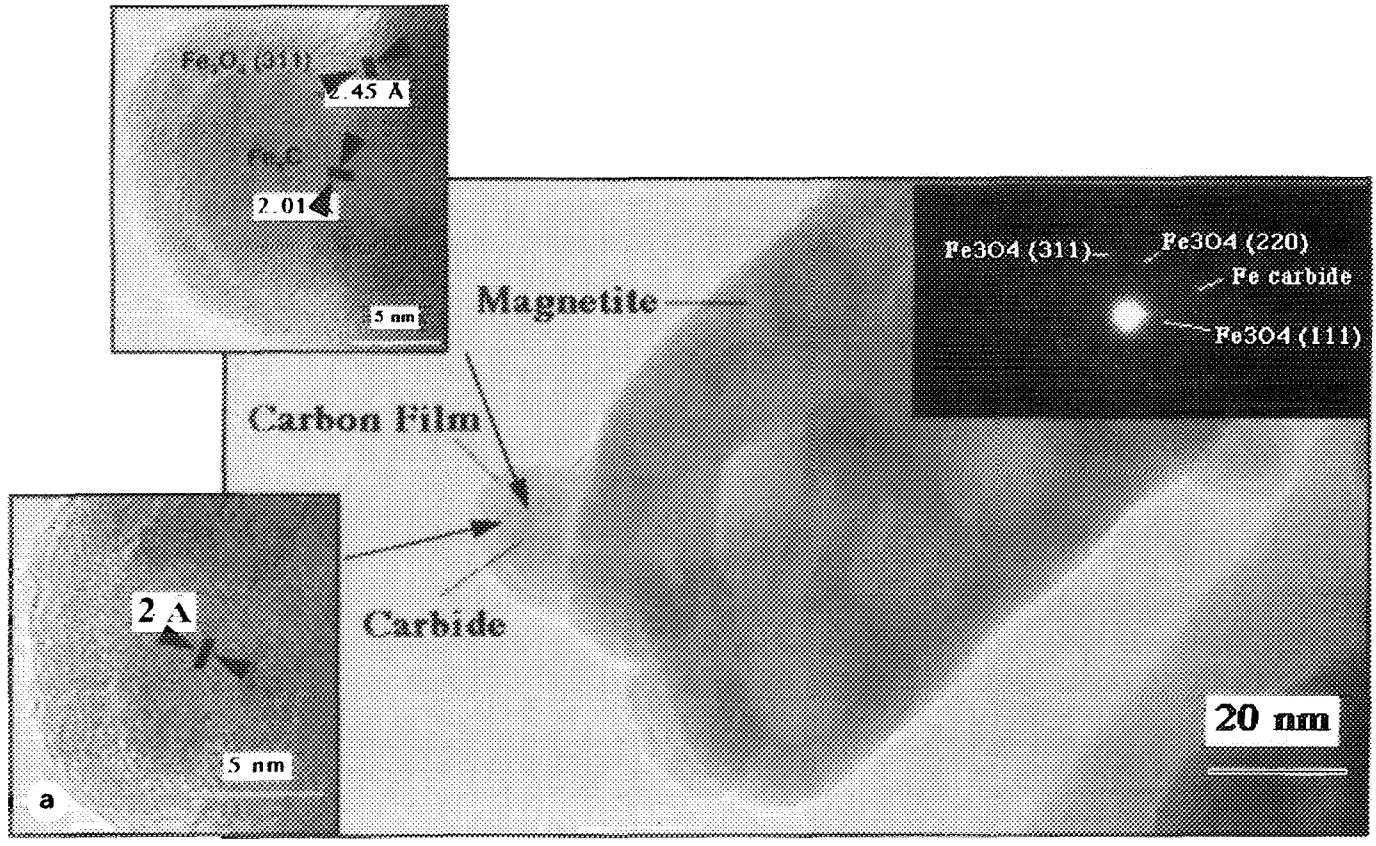

FIG. 15. TEM view of the catalyst after activation treatments shown in Fig. 14 followed by Fischer–Tropsch reaction (H_2/CO ratio = 0.7) for 10 h. (a) Sample initially activated in H_2 at 543 K. The insets show higher magnification views of the regions denoted by arrows. Electron diffraction shows the catalyst to contain both the magnetite and carbide phases. (b) Sample initially activated in CO at 543 K. The electron diffraction and the high magnification inset show the catalyst to contain both the magnetite and the carbide phases. (c) Sample initially activated in syngas mixture at 523 K. The electron diffraction and the high magnification inset show the catalyst to contain both the magnetite and the carbide phases.

$$S = \frac{2LW + 2(L + W)d}{\rho LWd}$$
$$S \approx \frac{2}{\rho d}, \qquad [8]$$

when $d \ll L, W$. Based on these equations, a BET surface area of 27 m^2/g corresponds to a thickness of about 15 nm for particles of density 4.7 g/cm^3 (from helium pycnometry). However, the observed thickness of the crystallites is about 40–50 nm, which is greater than the calculated value. The discrepancy is probably due to the swiss cheese morphology of the single crystals which may serve to enhance the surface area beyond the value calculated from the geometry of the particles.

During reaction, the hematite breaks down into carbide crystallites that are 20–30 nm in diameter. The surface area of the catalyst after reaction (21–24 m^2/g) is not very different from the original surface area. This surface area is consistent with spherical particles of diameter 38–34 nm and density 7.4 g/cm^3 (carbide) (26), in agreement with particle sizes observed by HRTEM. The BET surface area does not change significantly as the catalyst is activated and used for reaction. Since the BET surface area includes contributions from the oxide and carbide phases along with the possibility that the surface carbon overlayers are porous, the BET surface area does not serve as a good indicator of catalyst activity.

The Nature of the Active Phase

Our results indicate that the magnetite is not catalytically active, but transformation of the magnetite into carbide is a prerequisite to obtain FT activity. This is seen in the lack of initial methane formation on the samples activated in H_2 at 543 K and in syngas at 523 K, both of which had only magnetite at the end of the activation step. The CO activated sample was the only one that contained some carbide, and it shows a significant methane formation rate immediately after introduction of the syngas mixture. On

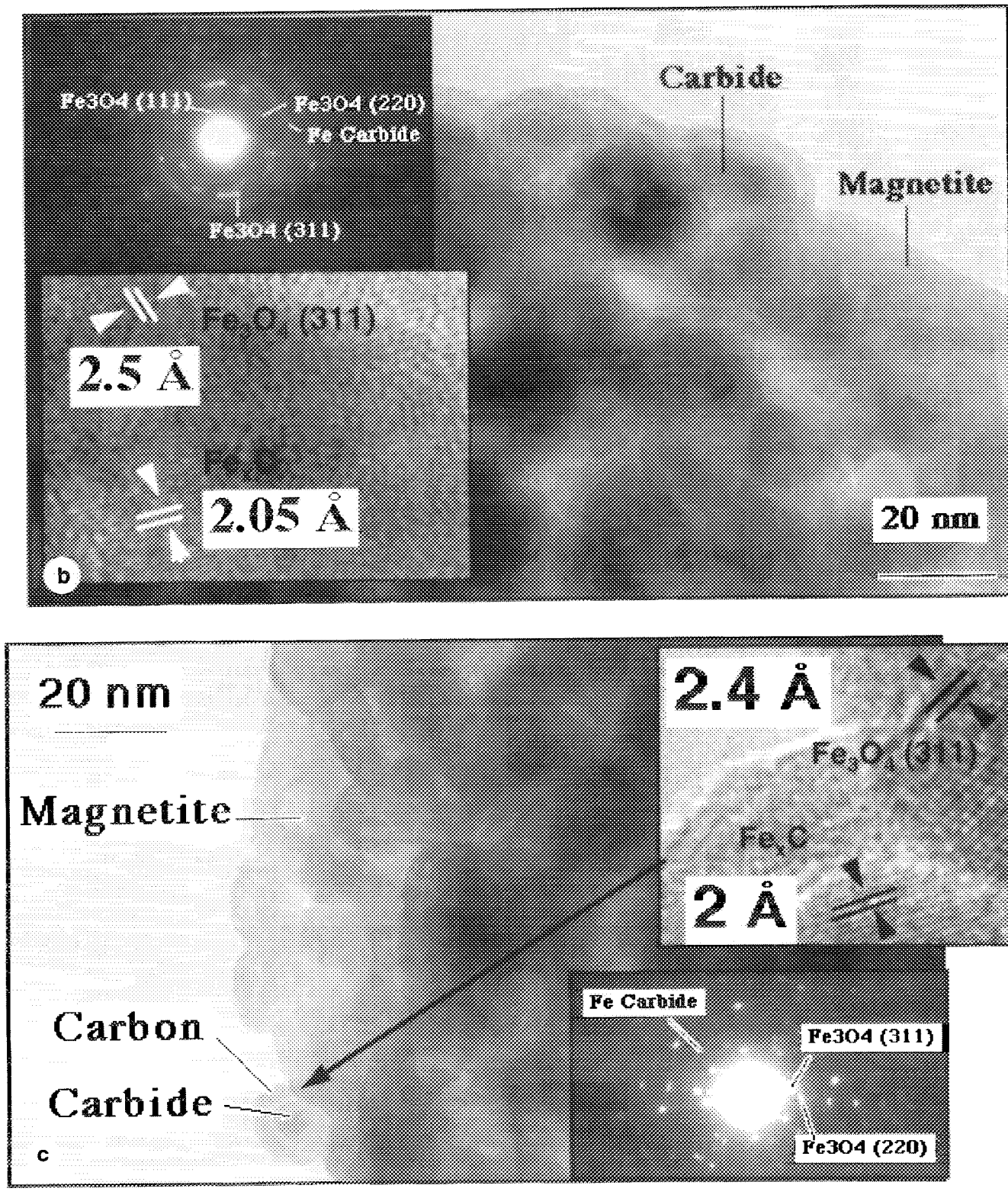

FIG. 15—*Continued*

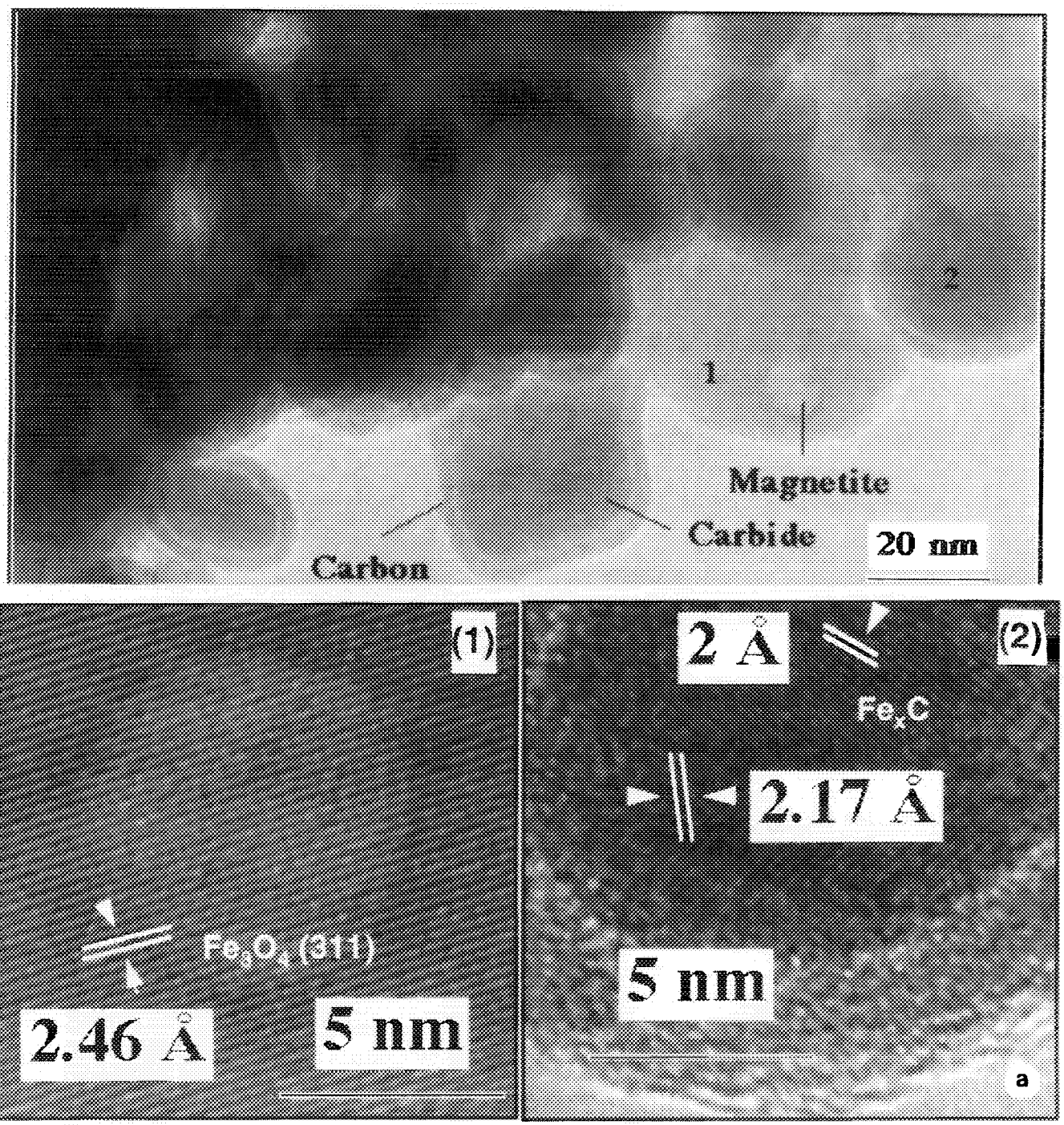

FIG. 16. TEM view of the catalyst after activation treatments shown in Fig. 14 followed by Fischer–Tropsh reaction (H_2/CO reactant ratio = 0.7) for 45 h. (a) Sample initially activated in H_2 at 543 K. The lower left corner of the picture is a high magnification view of the region marked "1" in the picture, which shows a magnetite particle, while the lower right corner of the picture is a high magnification view of the region marked "2" in the picture, which shows a carbide particle. (b) Sample initially activated in syngas mixture at 523 K. The carbide phase, the magnetite phase, and the carbon films are shown by markers. Electron diffraction and the high magnification inset show the presence of the carbide and the magnetite phase. (c) Sample initially activated in CO at 543 K. Electron diffraction and the high magnification inset show the carbide and the magnetite phases.

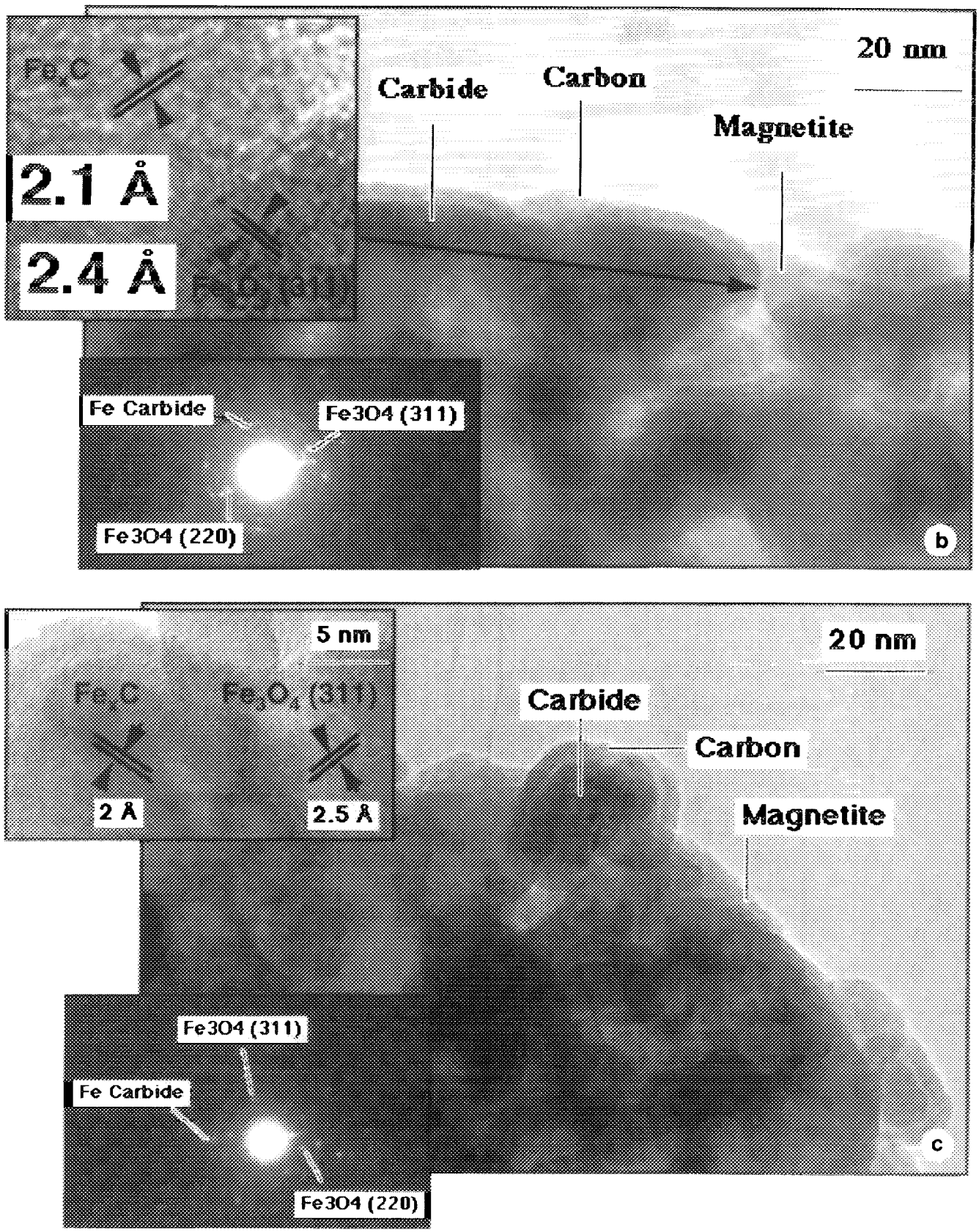

FIG. 16—*Continued*

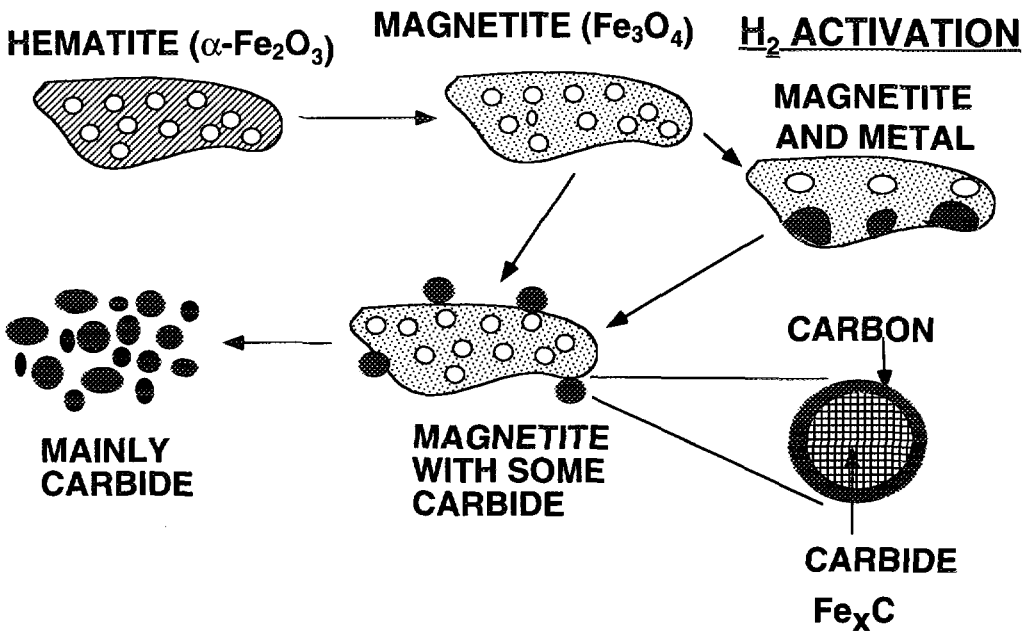

FIG. 17. Schematic representation of the morphological changes that accompany the phase changes that occur on the α-Fe_2O_3 catalyst as a result of activation and reaction conditions.

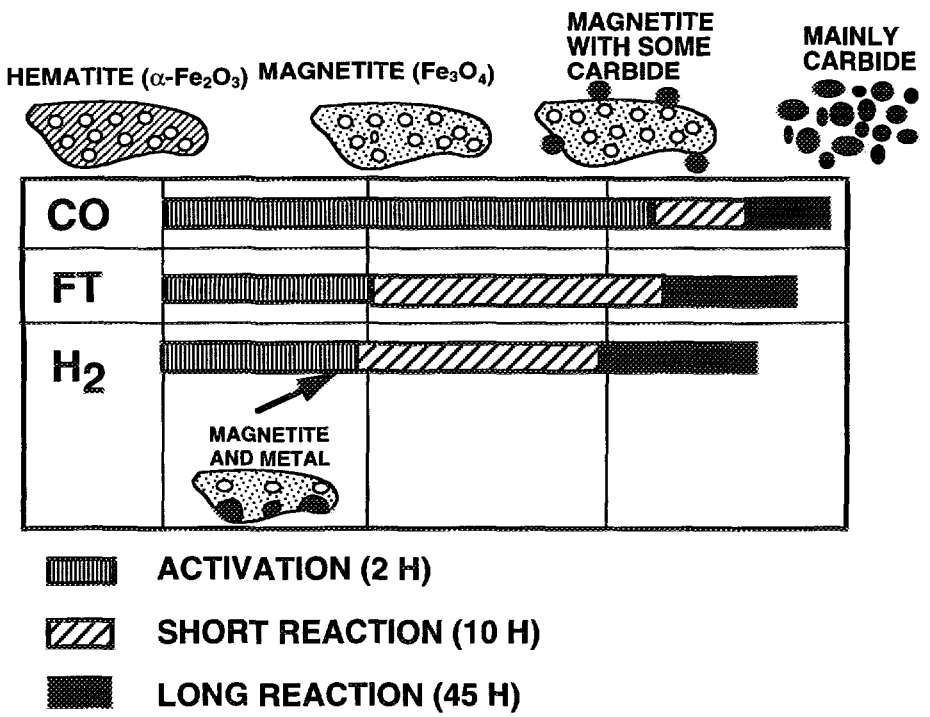

FIG. 18. Schematic representation of the differences in the extent of transformation caused by the different activation treatments.

the H_2 and syngas activated samples, the rate of methane formation is seen to increase commensurate with the slow increase in carbide formation, as seen in the TEM images, by XRD, and from the amount of carbon in the sample as measured by bulk CHN analysis. The transformation of magnetite to carbide does not seem to occur via the formation of a detectable metallic iron phase. This observation is consistent with that of Jung and Thomson on unsupported, unreduced iron oxide by *in situ* dynamic XRD (9), where metallic Fe was not detected during transformation of magnetite into carbide. This implies that if reduction of the oxide to the metal is a necessary step before carbide formation, the Fe metal must be present as a transient intermediate that is not detected by XRD or TEM.

Based on the TEM and XRD results, we cannot specify the stoichiometry of the carbide phase that is formed on our catalyst. If the active phase was χ–$Fe_{2.5}C$, we would expect to see approximately 7.9 wt% carbon in the sample. After a 10-h reaction with the CO activated sample, we have 6.85 wt% C and the sample still contains some magnetite as seen by XRD and TEM. The peak activity for methanation is achieved at this point. Therefore, our data would be consistent with the χ–$Fe_{2.5}C$ being the active phase in these catalysts. The CO-activated sample showed some deactivation after 45 h which was accompanied by an increase in carbon content. This suggests that carbonaceous layers deposited on the sample (as seen in TEM images) may slow down the reaction.

The initial low activity of the catalysts activated in H_2 and in syngas can be related to smaller extents of carbide formation. Even after 45 h on stream, the H_2-activated sample contains 6.2 wt% C while the syngas activated sample contains 5.1 wt% C, which suggests that both samples have still not completely transformed into the carbide. This observation is confirmed by TEM and XRD which show larger amounts of magnetite present on these samples than for the CO-activated sample. The amount of carbon seen by bulk elemental analysis and the extent of carbide formation seen by TEM and XRD was the lowest in the case of the isothermal syngas reaction at 523 K. This suggests that the higher temperature 543 K treatment may be necesssary to accelerate the solid-state transformation from magnetite into carbide.

Our conclusion that the transformation of magnetite into carbide is necessary to obtain FT synthesis activity in iron catalysts is consistent with the competition model proposed by Niemantsverdriet *et al.* (11, 27). This model states that the initial low activity of metallic iron is due to rapid diffusion of carbon atoms into the iron to form carbide, thereby removing carbon atoms from the surface and rendering them unavailable for FT reactions. As bulk carbiding approaches completion, the rate of diffusion of carbon decreases and the amount of carbon available on the surface for FT reactions increases. Within this model, the bulk carbide is not necessarily the active phase, but carbide formation must occur before the catalyst surface can retain enough carbon to become active. Similar arguments can explain the effects of the magnetite-to-carbide transformation on the FT activity of the catalyst studied in this work. The H_2-activated catalyst consists primarily of magnetite, which is inactive for FT. Upon exposure to the syngas mixture, CO is initially consumed mainly by conversion of magnetite to carbide. Once carbide is formed, any additional CO dissociation could result in FT synthesis products. Consequently, FT activity increases with the extent of transformation of magnetite into carbide. For the CO activated catalyst, carbide formation has already occurred to some extent prior to introduction of syngas, and the surfaces of these precarbided particles are active for FT synthesis immediately upon introduction of the syngas mixture. Ultimately, the buildup of inactive, graphitic carbon on the carbide particle surfaces inhibits the FT reaction and activity begins to decrease, resulting in the observed maximum in FT activity. Based on the TEM and activity results and the proposed model, nothing can be said about the nature of the active sites on the surface of the carbide particles, except that the formation of bulk carbide is necessary before the active site can be formed.

Huang *et al.* (16) found that Fe_3O_4 is the only crystalline phase detected by XRD at the point of maximum activity. However, they also show that Fe_3O_4, which is the only phase present after syngas activation, is inactive. Based on this evidence, they suggest the possibility of an active surface phase being formed on bulk Fe_3O_4. Our TEM results provide direct evidence of such a surface phase. Indeed, the surfaces of the small carbide nodules growing on the Fe_3O_4 surface constitute the active phase. Since the carbide particles supporting the catalytically active phase are present in small domains, their detection by bulk techniques like XRD may be difficult. A further complication is that the carbide and magnetite peaks overlap at around 43–45°, making their resolution difficult. In the XRD patterns of Huang *et al.* (16) unexpectedly high intensity in the peak at 43° is attributed to FeO, whereas we attribute this intensity to a carbide phase. This inference can be seen on comparing the ratio of the area of the peak at 43° with the primary magnetite peak at 35.5°, as shown in Table 2. It should also be noted that as a result of high H_2O and CO_2 partial pressures, Fe_3O_4 may be more prevalent at the higher conversions and operating pressures used by Huang *et al.* (16) than at the low pressures and conversions used in this study.

After performing FT synthesis on an unreduced iron oxide catalyst, Kuivila *et al.* (13) observed 22% carbide in the bulk of Mössbauer spectroscopy, but only ~3% carbide on the surface by XPS, and therefore concluded that a subsurface carbide phase had formed beneath a magnetite surface layer. Based in part on this result, they conclude

that magnetite is the active phase for FT synthesis. Reymond *et al.* (6) also observed substantial amounts of carbide by XRD, but little or no carbide by XPS. Our observation of a 3–4 nm thick carbon layer on the carbide phase, but not on the magnetite, allows a reinterpretation of the data in these two papers that does not require the counterintuitive concept of carbide formation beneath an oxide layer. In the presence of this carbon layer, the Fe 2*p* photoelectrons from the carbide would be attenuated by a factor of $\exp(-d/\lambda) = 0.07$ to 0.13, where $\lambda = 1.5$ nm is the attenuation length of Fe 2*p* photoelectrons (24) and $d =$ 3 to 4 nm is the carbon layer thickness. Since the magnetite signal is unattenuated (no carbon buildup occurs on the magnetite phase), a bulk composition of 22% carbide would result in an apparent surface composition of only ~2–4% carbide as measured by XPS, exactly as observed by Kuivila *et al.* (13) and consistent with our results and the qualitative results of Reymond *et al.* (6). Thus, measurement of low carbide signals by XPS cannot be interpreted to mean that carbide is absent from the catalyst surface, and therefore not an important phase in FT synthesis. Indeed, the difficulties involved in using XPS to detect carbide in the presence of oxide means that for partially carbided iron catalysts, XPS is not likely to shed any light on the chemical state of iron at the surface of the carbide particles. For a fully carbided catalyst, however, where the entire Fe 2*p* signal arises from the carbide particle surfaces, XPS could still prove useful in elucidating the nature of the iron at the surface of the particles. We find that when the carbon overlayer is removed by Ar^+ ion bombardment, the underlying carbide phase can indeed be detected by XPS (28).

The conclusion of Kuivila *et al.* (13) that magnetite and not carbide is catalytically active also contradicts their findings of lower, but not zero, FT activity of the metallic Fe catalyst. The metallic Fe catalyst has undoubtedly no magnetite to start with. In their experiments, the CO turnover frequency seems to correlate well with the extent of carbide information in agreement with our observations that methanation activity follows the increase in carbide content.

CONCLUSIONS

We have studied the role of various phases that are formed when an unsupported, precipitated iron oxide catalyst is activated for the Fischer–Tropsch synthesis reaction. Our study shows that during activation, the iron oxide transforms from hematite to magnetite and finally into an iron carbide phase. As the carbide content of the catalyst increases, we see the development of FT activity as measured by the rate of methane formation and CO consumption. Neither magnetite nor hematite were found to have any FT activity. Based on this correlation between carbide formation and activity, we conclude that carbide formation is necessary before iron FT catalysts can exhibit any activity. The exact nature of the surface phase on which the reaction takes place remains elusive, however, due to an inability of surface-sensitive techniques such as XPS to penetrate an amorphous carbon film which forms on the carbide particles during FT synthesis. These amorphous carbon films may hinder diffusion of the reactants to the catalyst surface, leading to eventual deactivation of the catalyst after long periods of reaction, and providing an explanation for the observation that the catalyst activity first increases and then starts to fall while the carbide content is still increasing. The formation of the carbide phase activates the catalyst while the simultaneous buildup of carbon on the carbide leads to deactivation.

The phase transformations in the catalyst play an important role in determining the activity, attrition resistance, and deactivation of this catalyst. Activation of this precipitated catalyst transforms single crystals to hematite to smaller crystallites of carbide. While the transformation from hematite to magnetite is extremely rapid, the magnetite-to-carbide transition is much slower under the conditions of temperature and pressure employed in our study. As carbon deposits on the carbide particles, it serves to further pry the carbide particles apart. In a commercial slurry phase reactor the convection currents could cause the carbide particles to break away, leading to catalyst attrition. The implication of this work for the attrition resistance of iron FT catalysts will be explored in detail in a forthcoming publication (25).

Comparison of the various activation treatments indicates that CO activation is able to transform the iron oxide catalyst most rapidly into the carbide phase, and thereby results in the most active catalyst. H_2 reduction to metallic iron may not necessarily be desirable since it causes the sulfur impurities to segregate to the catalyst surface, but partial reduction to magnetite in the presence of H_2 results in an active catalyst after an induction period required for carbide formation. The slowest activation was seen in syngas at reaction temperature (523 K), suggesting that activation at 543 K may be necessary to obtain higher catalyst activities at short times.

The conclusions of this study are based on spectroscopic analyses performed after cooling the catalyst to room temperature and transferring in air for analysis. Therefore, the results are subject to the limitations inherent in any room-temperature spectroscopic examination. We have performed very careful and controlled passivation of these catalysts to ensure that their microstructure was preserved during transfer in air for analysis. Hence, we are confident that the results are meaningful for understanding the behavior of unsupported, precipitated iron catalysts.

ACKNOWLEDGMENTS

We acknowledge financial support for the University of New Mexico portion of this study from Sandia National Laboratories and from the Petroleum Research Fund of the American Chemical Society (21168-AC5). Electron microscopy was performed at the Microbeam Analysis Facility within the department of Earth and Planetary Sciences, University of New Mexico. Sandia National Laboratories is funded by the United States Department of Energy under Contract DE-AC04-94AL85000.

REFERENCES

1. Fischer, F., and Tropsch, H., *Brennst. Chem.* **4,** 276 (1923).
2. Anderson, R. B., *in* "Catalysis" (P. H. Emmett, Ed.), Vol. IV, pp. 29–255. Van Nostrand-Reinhold, New York, 1956.
3. Jager, B., work presented at the Worldwide Industry Conference CatCon '94, Philadelphia, June 1994.
4. Bukur, D. B. "Development of improved Iron Fischer-Tropsch Catalysts," DOE/PC/89868, pp. IV-60. February 28, 1994.
5. Blanchard, F., Reymond, J. P., Pommier, B., and Teichner, S. J., *J. Mol. Catal.* **17,** 171 (1982).
6. Reymond, J. P., Meriaudeau, P., and Teichner, S. J., *J. Catal.* **75,** 39 (1982).
7. Raupp, G. B., and Delgass, W. N., *J. Catal.* **58,** 361 (1979).
8. Jung, H., and Thomson, W. J., *J. Catal.* **134,** 654–667 (1992).
9. Jung, H., and Thomson, W. J., *J. Catal.* **139,** 375–382 (1993).
10. LeCaer, G., Dubois, J. M., Pijolat, M., Perrichon, V., and Bussiere, P., *J. Phys. Chem.* **86,** 4799 (1982).
11. Niemantsverdriet, J. W., van der Kraan, A. M., van Dijk, W. L., and van der Baan, H. S., *J. Phys. Chem.* **84,** 3363 (1980).
12. Dictor, R. A., and Bell, A. T., *J. Catal.* **97,** 121 (1986).
13. Kuivila, C. S., Stair, P. C., and Butt, J. B., *J. Catal.* **118,** 299 (1989).
14. Butt, J. B., *Catal. Lett.* **7,** 61 (1990).
15. Butt, J. B., *Catal. Lett.* **7,** 83 (1990).
16. Huang, C.-S., Xu, L., and Davis, B. H., *Fuel Sci. Technol. Int.* **11,** 639 (1993).
17. Smith, J. M., and Van Ness, H. C., "Introduction to Chemical Engineering Thermodynamics," 4th ed. McGraw Hill, New York, 1987.
18. Messner, A. E., Rosie, D. M., and Argbright, P. A., *Anal. Chem.* **31,** 230 (1959).
19. Sault, A. G., *J. Catal.* **140,** 121 (1993).
20. Joint Committee for Powder Diffraction Standards, "JCPDS." International Center for Diffraction Data, 1979.
21. Kuivila, C. S., Butt, J. B., and Stair, P. C., *Appl. Surface Sci.* **32,** 99 (1988).
22. Sault, A. G., *Appl. Surface Sci.* **74,** 249 (1994).
23. Davis, L. E., McDonald, N. C., Palmberg, P. W., Riach, G. E., and Weber, R. E., "Handbook of Auger Electron Spectroscopy." Perkin-Elmer Corp., Eden Prairie, MN, 1978.
24. Seah, M. P., *in* "Practical Surface Analysis by Auger and X-ray Photoelectron Spectroscopy" (D. Briggs and M. P. Seah, Eds.), p. 181. Wiley, New York, 1983.
25. Kalakkad, D. S., Shroff, M. D., Kohler, S. D., Jackson, N. B., Sault, A. G., and Datye, A. K., submitted.
26. Perry, R. H., and Chilton, C. H., eds., "Chemical Engineers Handbook," 5th ed. McGraw Hill, New York, 1973.
27. Niemantsverdriet, J. W., and van der Kraan, A. M., *J. Catal.* **72,** 385 (1981).
28. Shroff, M. D., Kalakkad, D. S., Harrington, M. S., Jackson, N. B., Coulter, K. E., Sault, A. G., and Datye, A. K., "The Chemistry of Transition Metal Carbides" (S. T. Oyama, Ed.) Blackie, Glasgow/London, in press.